

Analysis of 26 Barium Stars $\star, \star\star$

II. Contributions of s-, r- and p-processes in the production of heavy elements

D.M. Allen $\star\star\star$ and B. Barbuy

Instituto de Astronomia, Geofísica e Ciências Atmosféricas, Universidade de São Paulo, Rua do Matão 1226, 05508-900 São Paulo, Brazil,
e-mail: dinah@astro.iag.usp.br, barbuy@astro.iag.usp.br

Received, 2006; accepted, 2006

ABSTRACT

Context. Barium stars show enhanced abundances of the slow neutron capture (s-process) heavy elements, and for this reason they are suitable objects for the study of s-process elements.

Aims. The aim of this work is to quantify the contributions of the s-, r- and p-processes for the total abundance of heavy elements from abundances derived for a sample of 26 barium stars. The abundance ratios between these processes and neutron exposures were studied.

Methods. The abundances of the sample stars were compared to those of normal stars thus identifying the fraction relative to the s-process main component.

Results. The fittings of the σN curves (neutron capture cross section times abundance, plotted against atomic mass number) for the sample stars suggest that the material from the companion asymptotic giant branch star had approximately the solar isotopic composition as concerns fractions of abundances relative to the s-process main component. The abundance ratios of heavy elements, hs, ls and s and the computed neutron exposure are similar to those of post-AGB stars. For some sample stars, an exponential neutron exposure fits well the observed data, whereas for others, a single neutron exposure provides a better fit.

Conclusions. The comparison between barium and AGB stars supports the hypothesis of binarity for the barium star formation. Abundances of r-elements that are part of the s-process path in barium stars are usually higher than those in normal stars, and for this reason, barium stars seemed to be also enriched in r-elements, although in a lower degree than s-elements. No dependence on luminosity classes was found in the abundance ratios behaviour among the dwarfs and giants of the sample barium stars.

Key words. barium stars – s-process – r-process – p-process

1. Introduction

Nucleosynthesis of elements benefited from the dispute between George Gamow and Fred Hoyle in explaining how the known chemical elements were formed (Alpher, Bethe & Gamow 1948; Hoyle 1946). Since then, our knowledge in primordial and stellar nucleosynthesis has greatly improved. Burbidge et al. (1957, B²FH) have based their work on solar abundances, and defined eight nucleosynthetic processes in stars, that would be responsible for the formation of the chemical elements. Wallerstein et al. (1997) presented a review of

B²FH, including recent and accurate experimental results and observations, where they showed that some processes defined by B²FH have been confirmed, others redefined and new processes not known by B²FH have been included in the list.

Three of the eight processes defined by B²FH will be focused in the present work, the s-, r- and p-processes. We present abundance ratios between these processes and abundance distribution for a number of heavy elements in a sample of barium stars. Abundance determination for the sample stars was described in Allen & Barbuy (2006, paper I hereafter).

The abundance ratios of best representatives of s- and r-processes provide clues on the knowledge of the formation and evolution of the Galaxy, since each of them is related to a different formation site, including stars of different characteristics and evolutionary stages. As an example, Mashonkina et al. (2003) estimated the timescale for the thick disk and halo formation based on abundance ratios of [Eu/Ba], [Mg/Fe] and [Eu/Fe], and on the calculations of chemical evolution by Travaglio et al. (1999). Burris et al. (2000) concluded, from abundances of metal-poor giant stars, that the contributions of

Send offprint requests to: D.M. Allen

* Based on spectroscopic observations collected at the European Southern Observatory (ESO), within the Observatório Nacional ON/ESO and ON/IAG agreements, under FAPESP project n° 1998/10138-8. Photometric observations collected at the Observatório do Pico dos Dias (LNA/MCT).

** Tables 2 and 6 are only available in electronic at the CDS via anonymous ftp to cdsarc.u-strasbg.fr/Abstract.html

*** Present address: Observatório do Valongo/UFRJ, Ladeira do Pedro Antonio 43, 20080-090 Rio de Janeiro, RJ, Brazil

s-processes can be seen at metallicities as low as $[\text{Fe}/\text{H}] = -2.75$, and they are present in stars of $[\text{Fe}/\text{H}] > -2.3$, indicating that the s-process acts at lower metallicities than predicted by previous work.

Considering the scenario of barium stars formation through enriched material transfer from a companion AGB star, it is worth to compare abundances of AGBs and barium stars. Such study can provide clues for the understanding of the enrichment in heavy elements of barium stars, given that they should conserve the surface characteristics of AGB stars.

This work intends to address the following questions:

1. What are the s-elements abundances of normal stars?
2. Considering the hypothesis of transfer of material enriched in carbon and s-elements from a more evolved companion for barium stars formation, is it possible to estimate in which proportion these elements are received, from observed abundances?
3. What is the isotopic composition of the material received? Is it possible to consider the solar system mix?
4. How is the σN curve behaviour for barium stars?
5. What kind of neutron exposures were involved in the nucleosynthesis of the transferred material?

This paper is organized as follows: Sect. 2 is a brief description of atmospheric parameters and abundance determination carried out in paper I; Sect. 3 explains briefly the s-, r- and p-processes; Sect. 4 shows the contributions of s-, r- and p-processes in normal stars compared with barium stars; Sect. 5 evaluates two kinds of neutron exposures and shows ratios involving s, hs and ls. In Sect. 6 conclusions are drawn.

2. Atmospheric Parameters and Abundance Calculations

The observations, atmospheric parameters and abundance calculations were described in detail in paper I. Here, we only outline the more important steps.

Photometric data were taken in several runs at the ZEISS 60cm telescope at LNA (Laboratório Nacional de Astrofísica) and from the literature. Optical spectra were obtained at the 1.52m telescope at ESO, La Silla, using the Fiber Fed Extended Range Optical Spectrograph (FEROS) (Kaufer et al. 2000). A set of atmospheric parameters (temperature, surface gravity, metallicities and microturbulent velocity) was obtained in an iterative way.

Photospheric 1D models were extracted from the NMARCS grid (Plez et al. 1992) for gravities $\log g < 3.3$, and from Edvardsson et al. (1993) for less evolved stars, with $\log g \geq 3.3$.

The LTE abundance analysis and the spectrum synthesis calculations were performed using the codes by Spite (1967, and subsequent improvements in the last thirty years), described in Cayrel et al. (1991) and Barbuy et al. (2003). Line lists and respective parameters are given in paper I.

3. s-, r- and p-Processes

Several important references describe in detail the s-, r- and p-processes: B²FH, Meyer (1994) and Wallerstein et al. (1997)

for a more general description, Käppeler et al. (1989), Busso et al. (1999), Lugaro et al. (2003), Lamb et al. (1977) and Raiteri et al. (1993) for the s-process, Woosley & Hoffman (1992), Wanajo et al. (2003) and Argast et al. (2004) for the r-process, Rayet et al. (1995) and Goriely et al. (2005) for the p-process, among others.

Typical s-elements are mainly produced by the s-process, but a smaller fraction of their abundance is due to the r-process. Analogously, the major production of r-elements is due to the r-process with a smaller contribution from s-process. Beyond these main processes, the p-process contributes with a small fraction of heavy elements production, as shown in Figure 1 of Meyer (1994).

In the s-process, neutrons are captured by seed nuclei, which are the iron peak elements, in a long timescale relative to β decay, denominated “s” (*slow*) by B²FH. This process has been subdivided into three components according to the site and the nucleosynthetic products: main, weak and strong.

The s-process main component is responsible by many isotopes in the range of atomic mass $63 \leq A \leq 209$. Abundance peaks can be observed near $A = 90, 138$ and 208 . In the classical analysis (Käppeler et al. 1989) the element formation through the s-process occurs in a chain, starting with the seed nucleus ^{56}Fe . Following this analysis, it is possible to obtain an expression for the σN , where σ is the neutron capture cross-section and N the abundances due to the s-process only for each nuclide. This expression involves the mean distribution of neutron exposure τ_o , the abundance fraction of ^{56}Fe required as seed to s-process G , and the solar abundance of ^{56}Fe N_{56}^{\odot} ,

$$\sigma_k N_k = \frac{GN_{56}^{\odot}}{\tau_o} \prod_{i=56}^k \left(1 + \frac{1}{\tau_o \sigma_i}\right)^{-1} \quad (1)$$

where k is the atomic mass number.

For the solar system, the corresponding curve from classical analysis represents very well the abundances of s-process nuclei for $A > 90$. For lighter nuclides, this line appears below the empirical data, suggesting another form of synthesis of s-process nuclides in stars, being the first one called main component and the second, weak component. The good agreement between the classical model and the observed data of this curve for the solar system represents an interesting characteristic of the s-process, taking into account the large number of nuclides between Fe and Bi.

The s-process main component is believed to occur during the thermal pulses - asymptotic giant branch (TP-AGB) phase of intermediate or low mass stars. In this phase, the star consists of an inert CO core and the He and H burning shells. The region between the two shells is the so-called He intershell, where neutrons released by the $^{13}\text{C}(\alpha, n)^{16}\text{O}$ reaction during the interpulse period, and by the $^{22}\text{Ne}(\alpha, n)^{25}\text{Mg}$ reaction during the convective thermal pulse, are captured by iron peak nuclei.

The s-process weak component is responsible for part of the abundance of nuclides with atomic mass in the range $23 \leq A \leq 90$ (Lamb et al. 1977; Raiteri et al. 1993). The nucleosynthetic site is likely the core helium burning of stars with masses $\geq 10 M_{\odot}$, where temperature is high enough for the main neutron

source to be the $^{22}\text{Ne}(\alpha, n)^{25}\text{Mg}$ reaction. Neutron density is low compared to the main component.

The s-process strong component was postulated in order to provide part of the Pb abundance (see Käppeler et al. 1989). However, according to Busso et al. (1999), it is possible to explain ^{208}Pb galactic abundance without it.

The r-process occurs in an environment rich in neutrons, where several of them are captured by nuclides in a short timescale compared to β decay, and for this reason, this process was denominated “r” (*rapid*) by B²FH. In this case, the neutron density is larger than that for the s-process. Sites that favour such high neutron density are final stages of massive stars as core collapse supernovae (SN II, Ib, Ic) (Wasserburg & Qian 2000; Qian 2000, 2001) or involving neutron stars (Woosley & Hoffman 1992; Meyer 1994; Freiburghaus et al. 1999; Rosswog et al. 1999, 2000).

The fact that r-elements are observed in very metal poor stars suggests that these elements were produced in supernovae events resulting from the evolution of the first massive stars in the Galaxy (Snedden et al. 1996, 2003; Hill et al. 2002; Cowan et al. 2002; Ishimaru et al. 2004; Honda et al. 2004). Despite these scenarios being promising, some difficulties are found, for instance, Wanajo et al. (2001) showed that to reproduce a solar abundance of r-elements, proto neutron stars must have 2 M_{\odot} and 10 km of radius, characteristics not observed so far.

The p-process forms nuclei rich in protons. Some s- or r-nuclei, where s- and r-processes were blocked, capture protons with γ emission (p, γ). The p-nuclei may also be synthesized by photodesintegration (γ, n) of a pre-existent nucleus rich in neutrons (especially s-nuclei), followed by possible cascades of (γ, p) and/or (γ, α) reactions.

The p-process site should be rich in hydrogen, with proton density $\geq 10^2$ g/cm³, at temperatures of $T = 2\text{--}3 \times 10^9$ K. This process site is likely related to SN II, according to Arnould (1976), Woosley & Howard (1978, and references therein), Arnould et al. (1992) and Rayet et al. (1993) or the explosion of a moderately massive white dwarf due to the accretion of He-rich matter (Goriely et al. 2005, and references therein). A quantitative study of the p-process is presented in Rayet et al. (1995).

4. Abundance distribution for s-, r- and p-processes

4.1. s-, r- and p-processes in normal stars

One way to quantify the enrichment of s-elements in barium stars is to compare their abundances with normal stars.

For the s-, r- and p-elements, the total abundance for the element can be described by the sum of the abundances corresponding to the three nucleosynthetic processes, taking into account all contributing isotopes “i”:

$$\epsilon(X) = \sum_i \epsilon_s^i + \sum_i \epsilon_r^i + \sum_i \epsilon_p^i.$$

In order to quantify the contribution of each process to the total abundance of several heavy elements in normal stars, an extensive set of stars from the literature was used. Peculiar

Table 1. Results obtained from least-squares fitting of $\log \epsilon_{nor}(X)$ vs. $[\text{Fe}/\text{H}]$ of normal stars: $\log \epsilon_{nor}(X) = A[\text{Fe}/\text{H}] + B$; ‘cov’ is the covariance between A and B; ‘dof’ is the number of degrees of freedom.

X	A	B	χ_{red}^2	cov (10^{-4})	dof
Sr	1.013 ± 0.024	2.908 ± 0.021	1.197	4.18	82
Y	1.112 ± 0.016	2.239 ± 0.013	1.002	1.58	160
Zr	0.939 ± 0.019	2.625 ± 0.015	1.385	2.06	66
Mo	0.970 ± 0.212	1.895 ± 0.342	1.472	715.2	7
Ba	0.992 ± 0.014	2.095 ± 0.011	1.978	1.07	214
La	1.190 ± 0.031	1.377 ± 0.039	4.891	10.91	47
Ce	1.009 ± 0.047	1.500 ± 0.047	0.923	20.20	34
Pr	0.867 ± 0.048	0.748 ± 0.050	1.180	19.99	13
Nd	0.950 ± 0.019	1.460 ± 0.017	1.635	2.46	99
Sm	0.811 ± 0.045	0.951 ± 0.045	1.407	18.76	34
Eu	0.783 ± 0.019	0.581 ± 0.015	1.263	2.20	165
Dy	0.840 ± 0.031	1.080 ± 0.044	4.312	11.70	22

Table 2. Abundances obtained from least-squares fittings for normal stars with metallicities corresponding to present sample barium stars. Each five lines correspond to the normal star with the same metallicity of the barium star indicated in parenthesis. $\log \epsilon(X)$ correspond to $\log \epsilon_{nor}(X)$ and $\epsilon_{s,r,p}(X)$ correspond to $\epsilon_{s,r,p}(X)_{nor}$ from equation 2. $\epsilon_o(X)$ is from equation 6. Full table is only available in electronic form.

	Sr	Y	Zr	Mo	Ba	La	Ce ...
	[Fe/H] = -0.06 (HD 749)						
$\log \epsilon(X)$	2.85 ± 0.18	2.17 ± 0.20	2.57 ± 0.17	1.84 ± 0.37	2.04 ± 0.18	1.31 ± 0.22	1.44 ± 0.19 ...
$\epsilon_s(X)$	594.4 ± 51.0	136.8 ± 63.2	307.4 ± 20.1	34.1 ± 29.2	87.7 ± 36.1	12.5 ± 6.3	20.9 ± 9.0 ...
$\epsilon_r(X)$	0.00 ± 0.00	11.9 ± 5.5	58.9 ± 23.0	17.9 ± 15.4	20.6 ± 8.5	7.7 ± 3.8	6.5 ± 2.8 ...
$\epsilon_p(X)$	109.0 ± 46.0	0.0 ± 0.0	4.1 ± 1.6	16.7 ± 14.3	0.2 ± 0.1	0.0 ± 0.0	0.1 ± 0.0 ...
$\epsilon_o(X)$	109.0 ± 46.0	11.9 ± 5.5	63.0 ± 24.6	34.6 ± 29.7	20.8 ± 8.6	7.7 ± 3.8	6.6 ± 2.8 ...
...

stars were withdrawn from these samples in order to obtain more reliable results. Figures 1 and 2 show the behaviour of the abundances ($\log \epsilon(X)$) of several heavy elements as a function of atmospheric parameters (T_{eff} , $\log g$, $[\text{Fe}/\text{H}]$). It is clear from these figures that $\log \epsilon(X)$ vs. $[\text{Fe}/\text{H}]$ is a linear correlation ($\log \epsilon_{nor}(X) = A[\text{Fe}/\text{H}] + B$), while $\log \epsilon(X)$ vs. T_{eff} and $\log g$ are not. Results of least-squares fittings for $\log \epsilon(X)$ vs. $[\text{Fe}/\text{H}]$ are shown in Table 1.

From $\log \epsilon(X)$ vs. $[\text{Fe}/\text{H}]$ fittings, it is possible to determine the total abundance of a certain element in a normal star of a given metallicity. The first line of Table 2 shows $\log \epsilon_{nor}(X)$ obtained directly from fittings for normal stars with metallicities corresponding to the barium star, indicated in the header. Data for molybdenum are rarely available in the literature in the same metallicity range as the present sample, and for this reason the least-squares fitting was done using data derived for the globular cluster ω Centauri by Smith et al. (2000), with results shown in column 2 of Table 3. In order to verify the reliability of these results, Mo abundances were calculated through $\log \epsilon_{nor}(\text{Mo}) = \log \epsilon_o(\text{Mo}) + [\text{Fe}/\text{H}] + [\text{Mo}/\text{Fe}]$, considering $[\text{Mo}/\text{Fe}] = 0$, and results are shown in column 3 of Table 3. The agreement between results from these two columns means

Table 3. Abundances [$\log \epsilon_{nor}(X)$] of Mo, Dy, Gd and Pb for normal stars. Symbol “*” indicates that the column was obtained from a least-squares fitting.

star	Mo*	Mo	Dy*	Dy	Gd	Pb
HD 749	1.84	1.86	1.03	1.14	1.06±0.19	1.89±0.20
HR 107	1.55	1.56	0.78	0.84	0.76±0.07	1.59±0.10
HD 5424	1.36	1.37	0.62	0.65	0.57±0.19	1.40±0.20
HD 8270	1.49	1.50	0.73	0.78	0.70±0.07	1.53±0.10
HD 12392	1.78	1.80	0.98	1.08	1.00±0.19	1.83±0.20
HD 13551	1.47	1.48	0.71	0.76	0.68±0.07	1.51±0.10
HD 22589	1.63	1.65	0.85	0.93	0.85±0.07	1.68±0.10
HD 27271	1.81	1.83	1.00	1.11	1.03±0.19	1.86±0.20
HD 48565	1.29	1.30	0.56	0.58	0.50±0.07	1.33±0.10
HD 76225	1.59	1.61	0.82	0.89	0.81±0.07	1.64±0.10
HD 87080	1.47	1.48	0.71	0.76	0.68±0.07	1.51±0.10
HD 89948	1.60	1.62	0.83	0.90	0.82±0.07	1.65±0.10
HD 92545	1.78	1.80	0.98	1.08	1.00±0.07	1.83±0.10
HD 106191	1.61	1.63	0.84	0.91	0.83±0.07	1.66±0.10
HD 107574	1.36	1.37	0.62	0.65	0.57±0.07	1.40±0.10
HD 116869	1.58	1.60	0.81	0.88	0.80±0.19	1.63±0.20
HD 123396	0.74	0.73	0.08	0.01	-0.07±0.19	0.76±0.20
HD 123585	1.43	1.44	0.68	0.72	0.64±0.07	1.47±0.10
HD 147609	1.46	1.47	0.70	0.75	0.67±0.07	1.50±0.10
HD 150862	1.80	1.82	1.00	1.10	1.02±0.07	1.85±0.10
HD 188985	1.60	1.62	0.83	0.90	0.82±0.07	1.65±0.10
HD 210709	1.86	1.88	1.05	1.16	1.08±0.19	1.91±0.20
HD 210910	1.54	1.55	0.77	0.83	0.75±0.19	1.58±0.20
HD 222349	1.28	1.29	0.55	0.57	0.49±0.07	1.32±0.10
BD+18 5215	1.38	1.39	0.63	0.67	0.59±0.07	1.42±0.10
HD 223938	1.56	1.57	0.79	0.85	0.77±0.19	1.60±0.20

that, according to the fitting, $[\text{Mo}/\text{Fe}] \approx 0$ at metallicities near solar. Data for Gd and Pb are also rare in the literature, for normal stars in the range of metallicities of the present sample, and for this reason, $\log \epsilon_{nor}(\text{Gd})$ and $\log \epsilon_{nor}(\text{Pb})$ were determined by considering $[\text{Gd}/\text{Fe}] = [\text{Pb}/\text{Fe}] = 0 \pm 0.05$, near the solar metallicity. Gd is expected to behave like Dy given that both are produced mainly through the r-process in almost the same proportions (Arlandini et al. 1999). Columns 4 and 5 of Table 3 show $\log \epsilon_{nor}(\text{Dy})$ values determined by least-squares fitting and by summing the star metallicity to the solar value, and columns 6 and 7 show $\log \epsilon_{nor}(\text{Gd})$ and $\log \epsilon_{nor}(\text{Pb})$.

Considering that the total abundance of an element is the sum of the contributions of s-, r- and p-processes, one can write:

$$\epsilon_{nor}(X) = \epsilon_s(X)_{nor} + \epsilon_{sw}(X)_{nor} + \epsilon_{st}(X)_{nor} + \epsilon_r(X)_{nor} + \epsilon_p(X)_{nor} \quad (2)$$

where $\epsilon_s(X)_{nor}$, $\epsilon_{sw}(X)_{nor}$ and $\epsilon_{st}(X)_{nor}$ are, respectively, the contributions of main, weak and strong components of s-process and $\epsilon_r(X)_{nor}$ and $\epsilon_p(X)_{nor}$ the r- and p-processes. Arlandini et al. (1999) provide detailed information about s-process main component and r-process. According to Lugaro et al. (2003), around 50% of ^{86}Sr and ^{87}Sr in the solar system

results from the s-process weak component, hence, the missing abundance which completes the total abundance in Arlandini et al. (1999) for these Sr isotopes was attributed to the weak component. 45% of ^{96}Zr abundance missing in Arlandini et al. was also attributed to the s-process weak component. A few nuclides are formed mainly through p-process, and they are not in Arlandini et al. (1999), such as ^{138}La , $^{136,138}\text{Ce}$, ^{144}Sm , $^{156,158}\text{Dy}$ (Rayet et al. 1995). The total solar abundances adopted by Arlandini et al. (1999) were those from Anders & Grevesse (1989), and it is possible to deduce the abundance of each nuclide p-only. For nuclides partially p, the difference between the total abundance and the sum of s- and r-fractions from Arlandini et al. (1999) was computed, such as for ^{94}Mo , ^{142}Nd , $^{152,154}\text{Gd}$ and ^{160}Dy . The isotopes $^{142,150}\text{Nd}$ are missing in Rayet et al. (1995), however they were considered p-partial or p-only according to the missing of part or total in Arlandini et al.. Once all abundance percentages were identified, it was possible to derive the abundance fractions of each process relative to total abundance of an element, shown in columns 3-7 of Table 4. The total abundance of each element taking into account its n isotopes for normal stars can be written as

$$\epsilon_{nor}(X) = \left(\sum_i^n g_s^i + \sum_i^n g_{sw}^i + \sum_i^n g_{st}^i + \sum_i^n g_r^i + \sum_i^n g_p^i \right) \epsilon_{nor}(X) \quad (3)$$

where g_s^i , g_{sw}^i , g_{st}^i , g_r^i and g_p^i are fractions of total abundance relative to the three s-process components, r- and p-processes, respectively, for each isotope “ i ”.

The uncertainty on $\log \epsilon_{nor}(X)$ is calculated with

$$\sigma_{\log \epsilon_{nor}(X)} = \left([\text{Fe}/\text{H}]^2 \sigma_A^2 + A^2 \sigma_{[\text{Fe}/\text{H}]}^2 + \sigma_B^2 + 2[\text{Fe}/\text{H}] \text{cov}(A, B) \right)^{0.5} \quad (4)$$

where $\text{cov}(A, B)$ is the covariance between A and B. The uncertainties on abundances relative to s-, r- and p-processes are given by

$$\sigma_{\epsilon_j} = \epsilon_j \sigma_{\log \epsilon_{nor}(X)} \ln 10 \quad (5)$$

where “ j ” corresponds to the process involved (s: main, sw: weak, st: strong, components of s-process, r: r-process, or p: p-process).

Finally, the sum of abundances from other processes except the s-process main component was computed, i.e., the sum of fractions sw, st, r and p, indicated by subscript “o” and its uncertainty are

$$\epsilon_o(X) = \left(\sum_i^n g_{sw}^i + \sum_i^n g_{st}^i + \sum_i^n g_r^i + \sum_i^n g_p^i \right) \epsilon_{nor}(X) \quad (6)$$

and

$$\sigma_{\epsilon_o(X)} = \epsilon_o(X) \sigma_{\log \epsilon_{nor}(X)} \ln 10. \quad (7)$$

Lines 2, 3 and 4 of Table 2 show abundances due to s-process main component, r- and p-process, respectively, and line 5 shows $\epsilon_o(X)$.

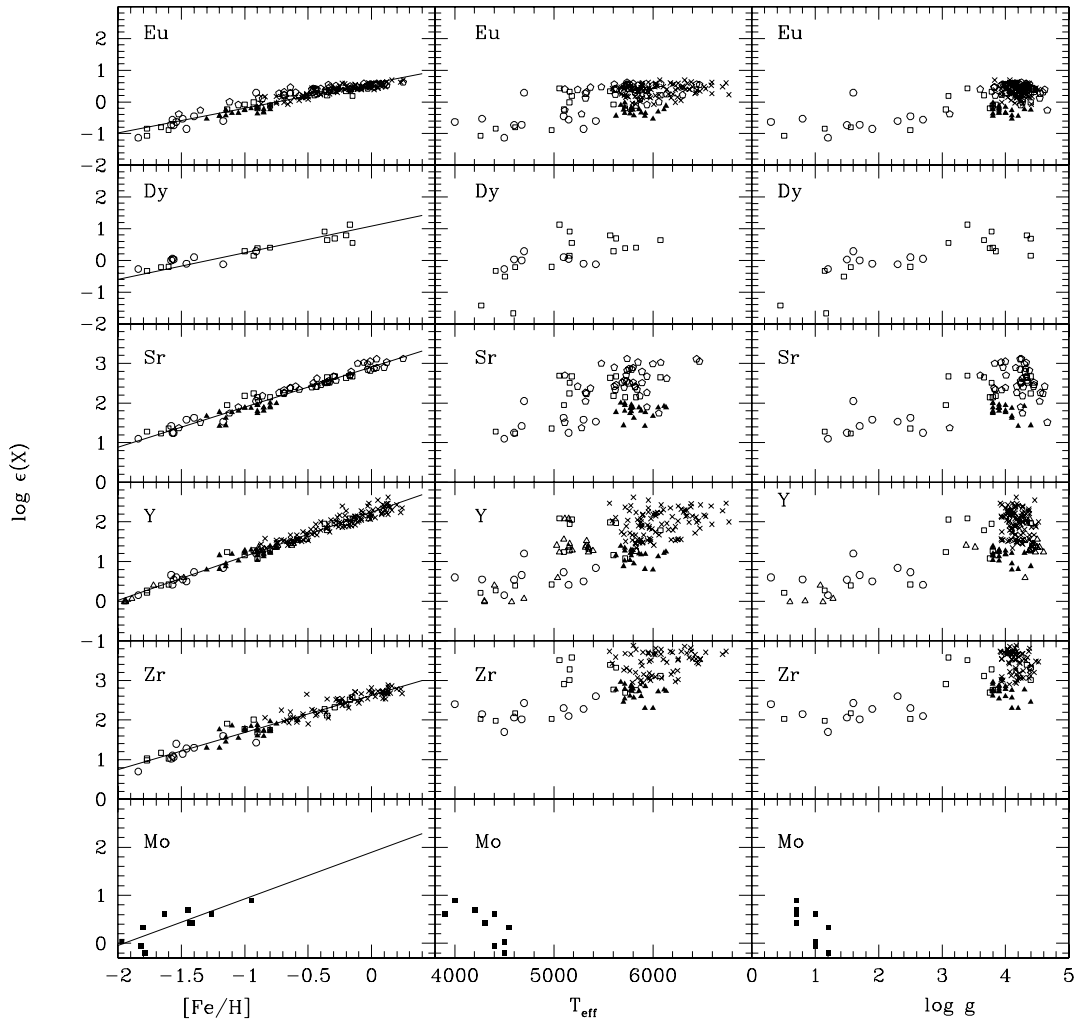


Fig. 1. $\log \epsilon(X)$ vs. atmospheric parameters ($[\text{Fe}/\text{H}]$, T_{eff} , $\log g$) for normal stars. Symbols indicate different references: open squares: Gratton & Sneden (1994); open circles: Burris et al. (2000); open triangles: Tomkin & Lambert (1999); filled triangles: Jehin et al. (1999); crosses: Edvardsson et al. (1993) and Woolf et al. (1995); filled squares: Smith et al. (2000); open pentagon Mashonkina & Gehren (2001). Uncertainties were taken from the respective references, otherwise, the values of ± 0.1 for $[\text{Fe}/\text{H}]$ and ± 0.05 for $\log \epsilon(X)$ were used. These values were also attributed to Jehin et al. (1999), given that their uncertainties seem underestimated.

4.2. *s*-, *r*- and *p*-processes in barium stars

Barium stars are enriched in neutron capture elements, and the excess of heavy elements can be deduced from a comparison with normal stars of similar metallicities. If the excess is due to the *s*-process main component, one can consider that abundances due to other processes (*r*, *p*, and other *s*-process components) are similar to those of normal stars of same metallicity, i.e., $\epsilon_r(X) = \epsilon_r(X)_{\text{nor}}$, $\epsilon_p(X) = \epsilon_p(X)_{\text{nor}}$, $\epsilon_{\text{sw}}(X) = \epsilon_{\text{sw}}(X)_{\text{nor}}$ and $\epsilon_{\text{st}}(X) = \epsilon_{\text{st}}(X)_{\text{nor}}$. In this way, $\epsilon_o(X)$ (line 5 of Table 2) was attributed to each barium star as the fraction corresponding to processes other than the *s*-process main component. The logarithmic mean abundances ($\log \epsilon(X)$) shown in Tables 13 and 14 of paper I were used to compute the fractions corresponding to each process.

The abundance fraction corresponding to the *s*-process main component of an element is

$$\epsilon_s(X) = \epsilon(X) - \epsilon_o(X). \quad (8)$$

Table 5 shows abundances relative to the *s*-process main component calculated with equation 8. In order to characterise the overabundance of neutron capture elements in barium stars, $\epsilon_s(X)$ values were compared to $\epsilon_s(X)_{\text{nor}}$ from Table 2, which is the fraction relative to the *s*-process main component in a normal star of same metallicity. Table 5 also shows the percentages $\epsilon_s(X)/\epsilon_s(X)_{\text{nor}} \times 100$. The *r*-elements, Sm, Eu, Gd and Dy, also show large overabundances, in some cases, similar to *s*-elements.

Normal stars are expected to have lower abundances of heavy elements than barium stars ($\epsilon_{\text{nor}}(X) < \epsilon(X)$), however,

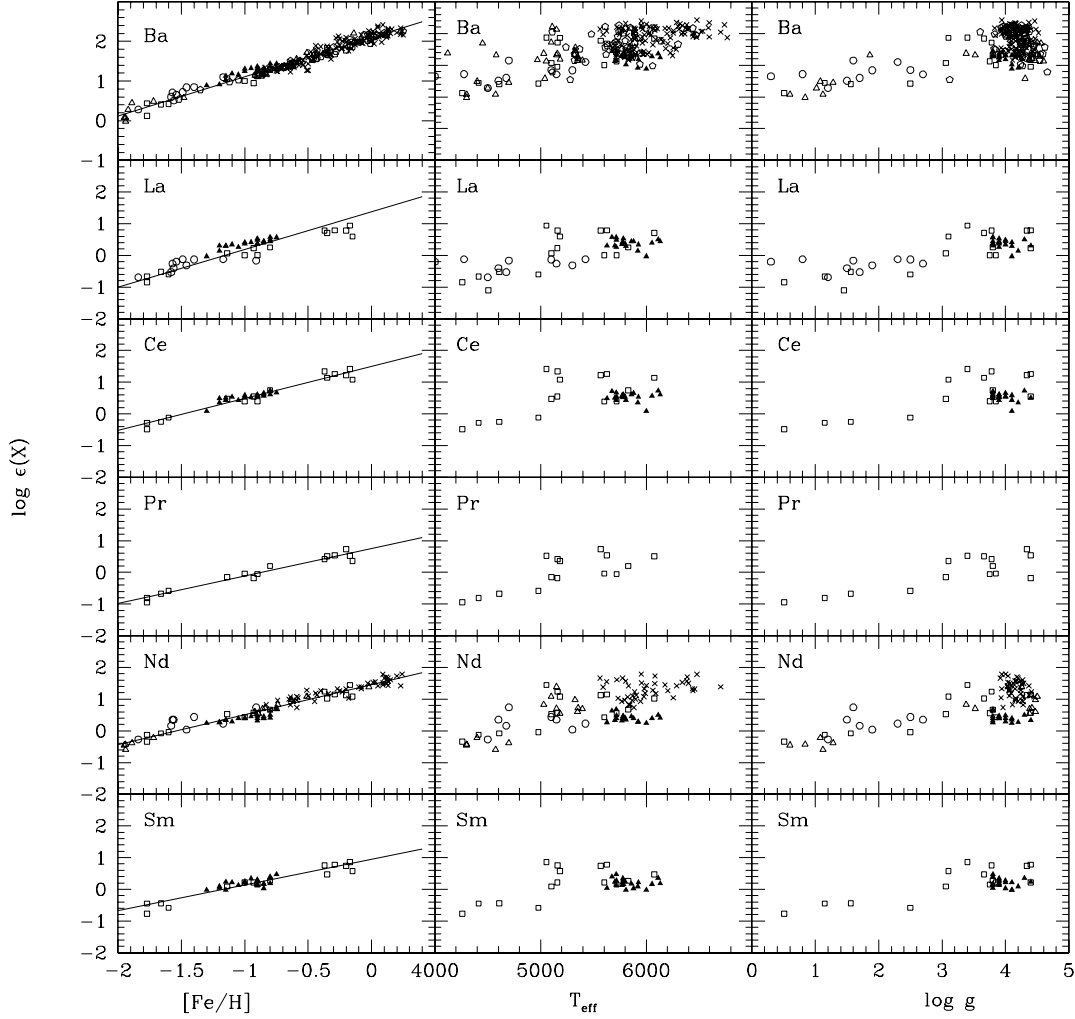


Fig. 2. Same as Figure 1 for other elements.

for some elements in some stars, abundances in barium stars obtained for the present sample were much lower than those of normal stars. It is the case of Mo (HD 27271, HD 116869, HD 123396, HD 210709, HD 210910, HD 223938), Eu (HR 107), Gd (HD 210709), Dy (HD 89948) and Pb (HD 22589, HD 210910). It is not clear why these barium stars show such low abundances of these elements. For these cases, the equation 8 does not apply, and there is no $\epsilon_s(X)$ for them (Table 5).

After computing the abundance relative to the s-process main component for an element in barium stars using equation 8, the abundance of each isotope and for each process can be determined with

$$\epsilon_s^i(X) = f_s^i \epsilon_s(X); \quad \sigma_{\epsilon^i s(X)} = f_s^i \sigma_{\epsilon_s(X)} \quad (9)$$

$$\epsilon_{sw}^i(X) = f_{sw}^i \epsilon_{sw}(X); \quad \sigma_{\epsilon^i sw(X)} = f_{sw}^i \sigma_{\epsilon_{sw}(X)} \quad (10)$$

$$\epsilon_{st}^i(X) = f_{st}^i \epsilon_{st}(X); \quad \sigma_{\epsilon^i st(X)} = f_{st}^i \sigma_{\epsilon_{st}(X)} \quad (11)$$

$$\epsilon_r^i(X) = f_r^i \epsilon_r(X); \quad \sigma_{\epsilon^i r(X)} = f_r^i \sigma_{\epsilon_r(X)} \quad (12)$$

$$\epsilon_p^i(X) = f_p^i \epsilon_p(X); \quad \sigma_{\epsilon^i p(X)} = f_p^i \sigma_{\epsilon_p(X)} \quad (13)$$

where f_s^i , f_{sw}^i , f_{st}^i , f_r^i and f_p^i are the abundance fractions of the corresponding isotope “i”, respectively, of the three s-process components, the r- and p-processes relative to total abundance of the involved process, shown in columns 8 to 12 of Table 4. The total abundance can be described by the equation

$$\epsilon(X) = \sum_i^n f_s^i \epsilon_s(X) + \sum_i^n f_{sw}^i \epsilon_{sw}(X) + \sum_i^n f_{st}^i \epsilon_{st}(X) + \sum_i^n f_r^i \epsilon_r(X) + \sum_i^n f_p^i \epsilon_p(X). \quad (14)$$

Abundances relative to the s-process main component for each nuclide of the sample barium stars are shown in column 3 of Table 6, and for normal stars, in column 13. The difference between these two columns is shown in column 15.

Some elements of Table 2 are formed in larger amount through the r-process. They are Eu (94.2%), Gd (84.54%), Dy (84.8%) and Sm (67.4%), according to Arlandini et al. (1999). For these elements, barium stars are expected to have abundances values closer to normal stars than for s-elements. It can

Table 5. Abundance fractions corresponding to the s-process main component for barium stars calculated with equation 8 (upper table) and percentage of abundance (lower table) relative to the s-process main component of a barium star compared to normal stars of a same metallicity ($\epsilon_s(X)/\epsilon_s(X)_{nor} \times 100$).

star	$\epsilon_s(\text{Sr})$	$\epsilon_s(\text{Y})$	$\epsilon_s(\text{Zr})$	$\epsilon_s(\text{Mo})$	$\epsilon_s(\text{Ba})$	$\epsilon_s(\text{La})$	$\epsilon_s(\text{Ce})$	$\epsilon_s(\text{Pr})$	$\epsilon_s(\text{Nd})$	$\epsilon_s(\text{Sm})$	$\epsilon_s(\text{Eu})$	$\epsilon_s(\text{Gd})$	$\epsilon_s(\text{Dy})$	$\epsilon_s(\text{Pb})$
HD 749	3781±2150	2260±994	9600±4450	63±64	1771±784	207±94	1364±600	28±18	512±241	70±35	3±3	14±21	106±74	144±126
HR 107	2237±791	294±28	614±74	127±45	512±60	24±4	53±7	5±1	20±4	6±2	...	16±5	...	288±135
HD 5424	1012±579	522±230	2517±1169	26±23	1132±498	131±58	1027±450	30±18	410±190	52±25	1.4±1.4	7±9	197±129	303±211
HD 8270	2790±980	580±54	1475±173	110±39	652±76	48±7	127±15	4±1	52±8	6±2	0.92±0.61	5±2	2±1	89±47
HD 12392	4179±2362	2147±944	6854±3182	169±118	3331±1465	406±181	1792±786	83±49	647±302	226±106	5±4	28±32	60±44	918±638
HD 13551	3366±1178	758±70	1481±174	176±58	704±82	45±7	144±17	5±1	50±8	8±2	0.33±0.47	13±4	3±1	85±45
HD 22589	3748±1318	619±58	2463±288	49±26	543±64	32±5	71±9	3±1	24±4	3±1	0.70±0.69	2±2	3±1	...
HD 27271	3177±1812	1075±475	3459±1620	...	816±365	51±26	182±82	9±7	67±36	16±10	2.4±2.8	10±17	12±14	109±100
HD 48565	2451±857	421±39	1462±170	53±20	620±72	77±11	474±55	13±2	136±19	20±4	0.59±0.42	13±4	16±3	467±209
HD 76225	8244±2868	1259±117	3524±410	142±50	1457±169	105±15	281±33	11±2	74±11	13±3	0.85±0.69	12±4	10±2	285±135
HD 87080	3366±1178	812±75	3196±371	61±24	1476±171	265±37	977±113	27±4	365±51	46±9	3.8±1.3	34±9	75±11	346±159
HD 89948	5506±1923	915±85	2078±244	112±42	651±76	54±8	125±15	7±1	56±9	10±3	0.33±0.58	6±3	...	76±44
HD 92545	3670±1300	563±53	1624±193	128±52	1113±130	47±7	147±18	7±1	46±8	8±3	2.4±1.2	5±3	7±2	302±148
HD 106191	2088±743	723±67	2352±275	114±43	515±61	28±4	102±12	14±2	36±6	11±3	0.55±0.64	11±4	10±2	179±90
HD 107574	3277±1144	442±41	978±115	175±56	1923±222	53±8	145±17	5±1	54±8	10±2	1.45±0.65	5±2	6±1	268±123
HD 116869	735±440	314±140	869±417	...	660±294	55±26	187±84	8±6	92±45	14±8	0.3±1.3	5±10	21±18	279±202
HD 123396	144±84	56±25	394±184	...	170±75	16±7	134±59	4±3	64±30	9±5	0.26±0.36	5±5	15±10	88±61
HD 123585	4987±1737	1248±115	2980±346	262±83	2716±314	199±28	804±93	30±4	236±33	51±10	5.9±1.7	12±4	19±3	1031±458
HD 147609	112924±4479	2291±211	5047±584	144±48	1755±203	203±28	768±89	25±4	204±29	42±8	4.8±1.5	25±7	24±4	173±83
HD 150862	3616±1283	1647±153	4128±482	177±67	1116±131	60±9	134±16	8±1	38±7	8±3	1.15±0.98	9±4	9±3	317±155
HD 188985	4358±1527	900±83	2957±345	112±42	1070±125	95±14	425±49	14±2	149±21	23±5	1.14±0.76	17±5	7±2	374±174
HD 210709	944±587	526±235	2158±1024	...	639±289	50±26	242±109	8±6	97±50	13±9	0.3±2.1	...	11±14	185±154
HD 210910	2807±1580	254±114	357±180	...	547±244	29±14	93±42	13±8	37±20	8±5	3.1±2.4	16±18	8±9	...
HD 222349	2442±945	439±185	1536±948	52±22	758±434	69±29	297±108	7±4	118±70	16±12	0.20±0.32	9±12	12±15	578±248
BD+18 5215	3880±1353	515±48	2072±241	111±37	1151±133	59±8	189±22	9±1	52±8	13±3	0.3±0.4	52±13	13±2	60±33
HD 223938	1654±853	418±41	2024±179	...	982±88	63±10	242±34	6±1	145±17	22±3	1.5±1.8	9±3	18±2	350±258

star	Sr(%)	Y(%)	Zr(%)	Mo(%)	Ba(%)	La(%)	Ce(%)	Pr(%)	Nd(%)	Sm(%)	Eu(%)	Gd(%)	Dy(%)	Pb(%)
HD 749	636	1652	3123	185	2020	1654	6526	1166	3650	2987	1508	795	6715	404
HR 107	758	464	382	728	1159	440	514	392	274	421	...	1755	...	1609
HD 5424	534	1337	2362	224	3955	4015	15334	3274	8525	5487	1657	1293	32236	2619
HD 8270	1087	1066	1045	724	1691	1029	1398	341	813	514	888	609	268	570
HD 12392	809	1830	2539	568	4357	3820	9851	3890	5253	10711	2604	1844	4262	2953
HD 13551	1374	1466	1096	1206	1912	1019	1664	439	821	671	334	1755	358	570
HD 22589	1029	775	1261	231	1000	452	553	183	276	176	513	142	317	...
HD 27271	573	849	1201	...	996	439	934	396	506	732	1280	595	804	326
HD 48565	1522	1290	1596	545	2542	2862	8336	1591	3306	2377	824	2621	2914	4749
HD 76225	2485	1746	1968	731	2942	1666	2404	756	915	910	673	1251	981	1422
HD 87080	1374	1570	2365	419	4011	5984	11296	2417	5971	3973	3848	4627	9942	2322
HD 89948	1621	1236	1136	560	1285	828	1042	497	671	676	259	606	...	369
HD 92545	710	480	601	430	1456	444	810	343	374	402	1336	342	483	972
HD 106191	601	953	1258	560	993	418	831	946	429	746	417	1093	1002	854
HD 107574	1729	1134	918	1532	6716	1604	2164	605	1118	1083	1773	943	1023	2322
HD 116869	227	447	496	...	1364	896	1641	559	1156	977	241	539	2257	1422
HD 123396	337	737	1474	...	2565	2817	8848	1743	5382	3318	1004	2514	8375	3328
HD 123585	2235	2673	2404	1964	8085	5023	10199	2859	4219	4747	6372	1755	2702	495
HD 147609	5400	4546	3815	1010	4879	4725	9087	2297	3414	3666	4903	3533	3192	1193
HD 150862	668	1334	1464	569	1395	534	702	356	298	388	623	542	613	972
HD 188985	1283	1216	1616	560	2112	1461	3552	903	1791	1547	881	1691	672	1820
HD 210709	152	365	672	...	696	381	1106	299	660	517	137	...	673	81
HD 210910	973	411	227	...	1267	533	914	986	512	606	2718	1808	982	...
HD 222349	1553	1380	1714	545	3176	2643	5333	958	2931	2008	282	1869	2203	6009
BD+18 5215	1954	1255	1862	930	3840	1717	2692	980	1041	1307	353	8625	1978	7596
HD 223938	547	642	1233	...	2173	1107	2274	454	1950	1629	1288	979	1988	495

be verified that this supposition is valid for Eu by comparing data from Tables 13 and 14 of paper I to those from Table 2. Figure 3 shows the behaviour of $\log \epsilon_{nor}(X)$ of normal stars calculated by least-squares fitting with $\log \epsilon(X)$ of barium stars, and Figure 4 shows the behaviour of $\log \epsilon(X)$ of barium stars with $\log \epsilon_o(X)$. It is important to point out that Figures 3 to 10, the elements were arranged in increasing order of contribution of the s-process main component, following Arlandini et al. (1999), Eu, Gd, Dy, Sm, Pb, Pr, Mo, Nd, La, Ce, Ba, Zr, Sr and Y. Behaviours tend to be approximately constant, however, Eu data are very close to a straight line with tangent = 1, differently from the other elements. The larger distance of the data from tangent = 1, the larger is the abundance of barium stars

as compared to normal stars. If the fraction corresponding to the s-process main component is withdrawn as in Figure 4, the behaviours of Eu, Gd and Dy are almost unaltered relative to Figure 3, however the change in ordinates due to the missing abundance is remarkable for the other elements.

Figure 5 shows the behaviour of $\log \epsilon_s(X)$ with $\log \epsilon_s(X)_{nor}$, which are the abundance fractions of the s-process main component of barium stars (equation 8) and normal stars of same metallicity, respectively. Differently from Figure 4, the changes in ordinates due to the missing fraction r in Eu, Gd and Dy abundances in Figure 5 are remarkable, in comparison with Figure 3. Figure 5 shows similar differences from tangent = 1 as Figures 3 and 4, making evident that the fraction s of

Table 6. Results relative to s-, r- and p-processes for barium stars. $\epsilon_s(X)$, $\epsilon_{sw}(X)$ and $\epsilon_{st}(X)$: abundance fractions of s-process main, weak and strong components; $\epsilon_r(X)$ and $\epsilon_p(X)$: abundance fractions of r- and p-processes; σ_N and $\sigma_N(\text{Si})$: cross section times abundance fraction corresponding to s-process main component taking into account the overabundance of barium stars in an usual scale and Si scale; $\epsilon_s(X)_{nor}$: abundance fractions of s-process main component for normal stars; diff: $\epsilon_s(X) - \epsilon_s(X)_{nor}$; $\sigma_{N_{gs}}$: cross section times abundance fraction corresponding to s-process main component without the overabundance of barium stars. Full table is only available in electronic form.

A	el	$\epsilon_s(X)$	$\sigma_{\epsilon_s(X)}$	$\epsilon_{sw}(X)$	$\epsilon_{st}(X)$	$\epsilon_r(X)$	$\sigma_{\epsilon_r(X)}$	$\epsilon_p(X)$	$\sigma_{\epsilon_p(X)}$	σ_N	σ_{σ_N}	$\epsilon_s(X)_{nor}$	$\sigma_{\epsilon_s(X)_{nor}}$	diff	$\sigma_N(\text{Si})$	$\sigma_{\sigma_N(\text{Si})}$	$\sigma_{N_{gs}}$
HD 749																	
84	Sr	4.2	1.8
86	Sr	208.7	118.7	37±16	13357	7621	32.80	13.85	175.89	0.373E+03	0.213E+03	0.324E+03
87	Sr	145.5	82.7	23±9	13387	7635	22.87	9.66	122.64	0.374E+03	0.213E+03	0.325E+03
88	Sr	3427.1	1948.9	45±19	21248	12127	538.70	227.51	2888.40	0.593E+03	0.339E+03	0.516E+03
89	Y	2260.2	994.0	11.9	5.5	42944	18935	136.79	63.17	2123.40	0.120E+04	0.529E+03	0.111E+04
90	Zr	4297.9	1992.2	53.0	20.7	90255	42711	137.63	53.75	4160.22	0.252E+04	0.119E+04	0.211E+04
91	Zr	1247.0	578.0	1.8	0.7	74821	36089	39.93	15.60	1207.09	0.209E+04	0.101E+04	0.175E+04
92	Zr	1854.7	859.7	4.2	1.6	61205	29325	59.39	23.20	1795.30	0.171E+04	0.820E+03	0.143E+04
94	Zr	2021.7	937.2	52565	24450	64.74	25.29	1956.98	0.147E+04	0.683E+03	0.123E+04
96	Zr	178.5	82.7	4.1±1.6	1910	890	5.72	2.23	172.75	0.533E+02	0.249E+02	0.445E+02

the abundance of barium stars leads the behaviour. The difference between the maximum and minimum values of the abundance fraction corresponding to the s-process main component of normal stars is $\Delta \log \epsilon_s(X)_{nor} \approx 1$ in the range of metallicities of the sample stars. For barium stars this difference is larger, $\Delta \log \epsilon_s(X) \approx 2$.

According to Figure 6, the abundance relative to the s-process main component of heavy elements is essentially independent of [Fe/H] for the present sample barium stars.

4.3. Abundance ratios involving s- and r-processes

The r-process is related to final stages of evolution of massive stars ($M > 8 M_{\odot}$) whereas the s-process main component occurs in AGB stars of low (1-3 M_{\odot}) or intermediate (4-8 M_{\odot}) masses. The timescale for stars to reach the SN II ($t < 10^8$ yr) stage is lower than that for stars to reach the AGB phase ($t > 10^8$ yr), therefore the first heavy elements ejected in the interstellar medium of the Galaxy, observed in very metal-poor stars, are expected to be mainly due to the r-process (Truran et al. 2002). The products of nucleosynthesis of AGB stars to the interstellar medium, particularly the s-process main component appeared latter.

In order to investigate when the s-process contribution starts, usually ratios involving s- and r-processes by using the best representatives of each one, Eu for r- and Ba for s-processes are studied. Figure 6 from Burris et al. (2000) shows the behaviour of Ba relative to Eu for normal stars of metallicities $-3 < [\text{Fe}/\text{H}] < +0.5$. From the moment that s-process starts to produce Ba, an increase on its abundance relative to Eu can be seen, since the s-process is responsible for $\sim 81\%$ of its production, according to Arlandini et al. (1999).

Figure 7 shows $\log \epsilon(X)$ vs. [Fe/H] for barium stars from the present sample and post-AGB stars from Reyniers et al. (2004) and van Winckel & Reyniers (2000). Abundances of post-AGBs are larger or similar to those of barium stars, except for Sm in one star. This is expected considering that barium stars were enriched by an AGB companion.

Figure 8 shows $\log \epsilon(\text{Eu})$ vs. $\log \epsilon(X)$, where X are heavy elements other than Eu, for the present sample barium stars and stars from the literature. From Nd to Y, for which the s-process

contribution is larger, barium stars and post-AGBs are clearly overabundant, located on the high abundance end.

In the Ba panel of Figure 8, the lowest values of $\log \epsilon(\text{Eu})$ corresponding to normal stars, are close to the upper line where [Ba/Eu] = -0.70, representing Ba production by r-process only (Mashonkina et al. 2003). As $\log \epsilon(\text{Eu})$ increases, data become closer to the lower line, where data are compatible with [Ba/Eu] values for the solar ratio. Both barium and post-AGB stars values are very different from the solar ratio line.

In Figure 9, the r-process fraction of Eu abundance [$\log(0.942\epsilon(\text{Eu}))$] correlates with the s-process main component abundance fraction of other elements in barium stars. In Figure 10, the r-process fraction of Eu is plotted against fractions of r-process of other elements, for data given in Table 2. In the latter, the correlation is linear, with no dispersion, indicating that the s-process main component contribution causes a scatter in earlier figures. This linear correlation in Figure 10 is expected, given that only the r part of the abundances for all involved elements were used. Sr was not included in this figure because it does not have an r-process contribution (see Table 4).

[X/Eu] vs. [Fe/H] for barium and post-AGB stars are shown in Table 7 and Figure 11. The star HD 210910 shows lower values of [X/Eu] for Y, Zr, Ba, La, Ce, Nd, Pr and Pb, reaching negative values for [Zr/Eu] = -0.18. The value of [Sr/Eu] is low for the star HD 123396, [Sr/Eu] = -0.1. This result is expected from Figure 6 of paper I, which shows that the stars HD 123396 and HD 210910 present the lowest values of [SrII/Fe] and [ZrII/Fe], respectively, and their [Eu/Fe] = 0.50 and 0.54, thus very close. For other stars, [X/Eu] is in the range of $0 \leq [X/Eu] \leq 1.3$. The post-AGBs are also mainly in this range, the lowest value being [Zr/Eu] = -0.01. For all elements, [X/Eu] vs. [Fe/H] is approximately constant in the range of metallicities of the sample stars.

For Mo, that has a contribution of 49.76% of the s-process main component, 26.18% of the r-process and 24.06% of the p-process, [Mo/Eu] are mainly in the range from -0.4 to 0.6. Relative to Ba, the values are lower, in the range $-1.5 \leq [\text{Mo}/\text{Ba}] \leq -0.35$. Regarding the ratios involving Pr, that has 49% of contribution from the s-process main component and 51% from the r-process, data are mainly in the ranges $-1.01 \leq [\text{Pr}/\text{Ba}] \leq -0.04$

Table 7. [X/Eu] (upper table) and [X/Ba] (lower table) for the barium stars.

star	[Sr/Eu]	[Y/Eu]	[Zr/Eu]	[Mo/Eu]	[Ba/Eu]	[La/Eu]	[Ce/Eu]	[Nd/Eu]	[Pr/Eu]	[Pb/Eu]
HD 749	0.35±0.21	0.85±0.12	1.12±0.14	-0.20±0.21	0.85±0.13	0.93±0.12	1.17±0.13	1.00±0.13	0.56±0.25	0.05±0.27
HR 107	0.71±0.18	0.56±0.10	0.53±0.10	0.56±0.16	0.91±0.11	0.63±0.10	0.37±0.10	0.28±0.10	0.48±0.18	0.86±0.22
HD 5424	0.14±0.21	0.57±0.12	0.89±0.14	-0.26±0.21	1.02±0.13	1.09±0.12	1.40±0.13	1.26±0.13	0.92±0.25	0.64±0.27
HD 8270	0.58±0.18	0.63±0.10	0.68±0.10	0.28±0.16	0.79±0.11	0.68±0.10	0.51±0.10	0.41±0.10	0.16±0.18	0.18±0.22
HD 12392	0.30±0.21	0.73±0.12	0.88±0.14	0.02±0.21	1.03±0.13	1.13±0.12	1.19±0.13	1.01±0.13	0.91±0.25	0.67±0.27
HD 13551	0.79±0.18	0.87±0.10	0.81±0.10	0.59±0.16	0.95±0.11	0.78±0.10	0.70±0.10	0.52±0.10	0.36±0.18	0.29±0.22
HD 22589	0.67±0.18	0.62±0.10	0.86±0.10	-0.01±0.16	0.67±0.11	0.49±0.10	0.24±0.10	0.11±0.10	0.06±0.18	-0.36±0.22
HD 27271	0.33±0.21	0.58±0.12	0.73±0.14	-0.35±0.21	0.57±0.13	0.41±0.12	0.35±0.13	0.22±0.13	0.18±0.25	0.00±0.27
HD 48565	0.69±0.18	0.66±0.10	0.84±0.10	0.15±0.16	0.94±0.11	1.04±0.10	1.25±0.10	0.96±0.10	0.74±0.18	1.00±0.22
HD 76225	1.01±0.18	0.92±0.10	1.01±0.10	0.35±0.16	1.10±0.11	0.97±0.10	0.81±0.10	0.52±0.10	0.50±0.18	0.60±0.22
HD 87080	0.34±0.18	0.45±0.10	0.69±0.10	-0.26±0.16	0.82±0.11	1.08±0.10	1.07±0.10	0.90±0.10	0.58±0.18	0.39±0.22
HD 89948	0.92±0.18	0.86±0.10	0.87±0.10	0.34±0.16	0.83±0.11	0.77±0.10	0.55±0.10	0.49±0.10	0.44±0.18	0.19±0.22
HD 92545	0.41±0.18	0.32±0.10	0.43±0.10	0.08±0.16	0.72±0.11	0.40±0.10	0.28±0.10	0.10±0.10	0.12±0.18	0.38±0.22
HD 106191	0.45±0.18	0.71±0.10	0.87±0.10	0.30±0.16	0.68±0.11	0.46±0.10	0.41±0.10	0.28±0.10	0.64±0.18	0.45±0.22
HD 107574	0.63±0.18	0.49±0.10	0.48±0.10	0.43±0.16	1.24±0.11	0.69±0.10	0.55±0.10	0.39±0.10	0.23±0.18	0.58±0.22
HD 116869	0.09±0.21	0.43±0.12	0.52±0.14	-0.36±0.21	0.86±0.13	0.80±0.12	0.74±0.13	0.70±0.13	0.48±0.25	0.69±0.27
HD 123396	-0.10±0.21	0.20±0.12	0.69±0.14	-0.70±0.21	0.80±0.13	0.77±0.12	1.12±0.13	1.05±0.13	0.70±0.25	0.70±0.27
HD 123585	0.38±0.18	0.51±0.10	0.53±0.10	0.17±0.16	0.96±0.11	0.82±0.10	0.86±0.10	0.58±0.10	0.48±0.18	0.72±0.22
HD 147609	0.85±0.18	0.83±0.10	0.82±0.10	-0.01±0.16	0.83±0.11	0.89±0.10	0.90±0.10	0.58±0.10	0.48±0.18	0.04±0.22
HD 150862	0.50±0.18	0.88±0.10	0.92±0.10	0.30±0.16	0.83±0.11	0.60±0.10	0.35±0.10	0.14±0.10	0.25±0.18	0.50±0.22
HD 188985	0.69±0.18	0.73±0.10	0.89±0.10	0.21±0.16	0.91±0.11	0.87±0.10	0.94±0.10	0.75±0.10	0.53±0.18	0.66±0.22
HD 210709	0.01±0.21	0.45±0.12	0.71±0.14	-0.38±0.21	0.65±0.13	0.60±0.12	0.66±0.13	0.55±0.13	0.31±0.25	0.37±0.27
HD 210910	0.32±0.21	0.00±0.12	-0.18±0.14	-0.73±0.21	0.45±0.13	0.20±0.12	0.11±0.13	0.01±0.13	0.32±0.25	-0.58±0.27
HD 222349	0.81±0.18	0.79±0.10	0.98±0.10	0.26±0.16	1.14±0.11	1.11±0.10	1.16±0.10	1.02±0.10	0.65±0.18	1.21±0.22
BD+18 5215	0.91±0.18	0.77±0.10	1.01±0.10	0.46±0.16	1.22±0.11	0.95±0.10	0.87±0.10	0.59±0.10	0.64±0.18	0.21±0.22
HD 223938	0.24±0.21	0.37±0.12	0.69±0.14	-0.45±0.21	0.85±0.13	0.67±0.12	0.67±0.13	0.71±0.13	0.20±0.25	0.60±0.27
star	[Sr/Ba]	[Y/Ba]	[Zr/Ba]	[Mo/Ba]	[Pb/Ba]	[Pr/Ba]	[Sm/Ba]	[Gd/Ba]	[Dy/Ba]	
HD 749	-0.50±0.20	0.00±0.10	0.27±0.13	-1.05±0.20	-0.80±0.26	-0.29±0.24	-0.25±0.13	-0.86±0.35	-0.26±0.23	
HR 107	-0.20±0.17	-0.35±0.07	-0.38±0.07	-0.35±0.14	-0.05±0.21	-0.43±0.17	-0.65±0.11	-0.40±0.12	...	
HD 5424	-0.88±0.20	-0.45±0.10	-0.13±0.13	-1.28±0.20	-0.38±0.26	-0.10±0.24	-0.21±0.13	-1.03±0.35	0.17±0.23	
HD 8270	-0.21±0.17	-0.16±0.07	-0.11±0.07	-0.51±0.14	-0.61±0.21	-0.63±0.17	-0.74±0.11	-0.86±0.12	-1.07±0.09	
HD 12392	-0.73±0.20	-0.30±0.10	-0.15±0.13	-1.01±0.20	-0.36±0.26	-0.12±0.24	-0.04±0.13	-0.94±0.35	-0.76±0.23	
HD 13551	-0.16±0.17	-0.08±0.07	-0.14±0.07	-0.36±0.14	-0.66±0.21	-0.59±0.17	-0.71±0.11	-0.61±0.12	-1.07±0.09	
HD 22589	0.00±0.17	-0.05±0.07	0.19±0.07	-0.68±0.14	-1.03±0.21	-0.61±0.17	-0.80±0.11	-0.85±0.12	-0.84±0.09	
HD 27271	-0.24±0.20	0.01±0.10	0.16±0.13	-0.92±0.20	-0.57±0.26	-0.39±0.24	-0.47±0.13	-0.63±0.35	-0.68±0.23	
HD 48565	-0.25±0.17	-0.28±0.07	-0.10±0.07	-0.79±0.14	0.06±0.21	-0.20±0.17	-0.34±0.11	-0.60±0.12	-0.60±0.09	
HD 76225	-0.09±0.17	-0.18±0.07	-0.09±0.07	-0.75±0.14	-0.50±0.21	-0.60±0.17	-0.82±0.11	-0.91±0.12	-1.06±0.09	
HD 87080	-0.48±0.17	-0.37±0.07	-0.13±0.07	-1.08±0.14	-0.43±0.21	-0.24±0.17	-0.36±0.11	-0.58±0.12	-0.34±0.09	
HD 89948	0.09±0.17	0.03±0.07	0.04±0.07	-0.49±0.14	-0.64±0.21	-0.39±0.17	-0.56±0.11	-0.74±0.12	-1.30±0.09	
HD 92545	-0.31±0.17	-0.40±0.07	-0.29±0.07	-0.64±0.14	-0.34±0.21	-0.60±0.17	-0.80±0.11	-0.90±0.12	-0.95±0.09	
HD 106191	-0.23±0.17	0.03±0.07	0.19±0.07	-0.38±0.14	-0.23±0.21	-0.04±0.17	-0.42±0.11	-0.48±0.12	-0.59±0.09	
HD 107574	-0.61±0.17	-0.75±0.07	-0.76±0.07	-0.81±0.14	-0.66±0.21	-1.01±0.17	-1.07±0.11	-1.35±0.12	-1.37±0.09	
HD 116869	-0.77±0.20	-0.43±0.10	-0.34±0.13	-1.22±0.20	-0.17±0.26	-0.38±0.24	-0.46±0.13	-0.80±0.35	-0.47±0.23	
HD 123396	-0.90±0.20	-0.60±0.10	-0.11±0.13	-1.50±0.20	-0.10±0.26	-0.10±0.24	-0.11±0.13	-0.49±0.35	-0.11±0.23	
HD 123585	-0.58±0.17	-0.45±0.07	-0.43±0.07	-0.79±0.14	-0.24±0.21	-0.48±0.17	-0.59±0.11	-1.24±0.12	-1.15±0.09	
HD 147609	0.02±0.17	0.00±0.07	-0.01±0.07	-0.84±0.14	-0.79±0.21	-0.35±0.17	-0.48±0.11	-0.77±0.12	-0.87±0.09	
HD 150862	-0.33±0.17	0.05±0.07	0.09±0.07	-0.53±0.14	-0.33±0.21	-0.58±0.17	-0.80±0.11	-0.80±0.12	-0.89±0.09	
HD 188985	-0.22±0.17	-0.18±0.07	-0.02±0.07	-0.70±0.14	-0.25±0.21	-0.38±0.17	-0.48±0.11	-0.66±0.12	-1.01±0.09	
HD 210709	-0.64±0.20	-0.20±0.10	0.06±0.13	-1.03±0.20	-0.28±0.26	-0.34±0.24	-0.43±0.13	-0.78±0.35	-0.58±0.23	
HD 210910	-0.13±0.20	-0.45±0.10	-0.63±0.13	-1.18±0.20	-1.03±0.26	-0.13±0.24	-0.58±0.13	-0.43±0.35	-0.69±0.23	
HD 222349	-0.33±0.17	-0.35±0.07	-0.16±0.07	-0.88±0.14	0.07±0.21	-0.49±0.17	-0.50±0.11	-0.81±0.12	-0.79±0.09	
BD+18 5215	-0.31±0.17	-0.45±0.07	-0.21±0.07	-0.76±0.14	-1.01±0.21	-0.58±0.17	-0.76±0.11	-0.31±0.12	-0.92±0.09	
HD 223938	-0.61±0.20	-0.48±0.10	-0.16±0.13	-1.30±0.20	-0.25±0.26	-0.65±0.24	-0.47±0.13	-0.85±0.35	-0.71±0.23	

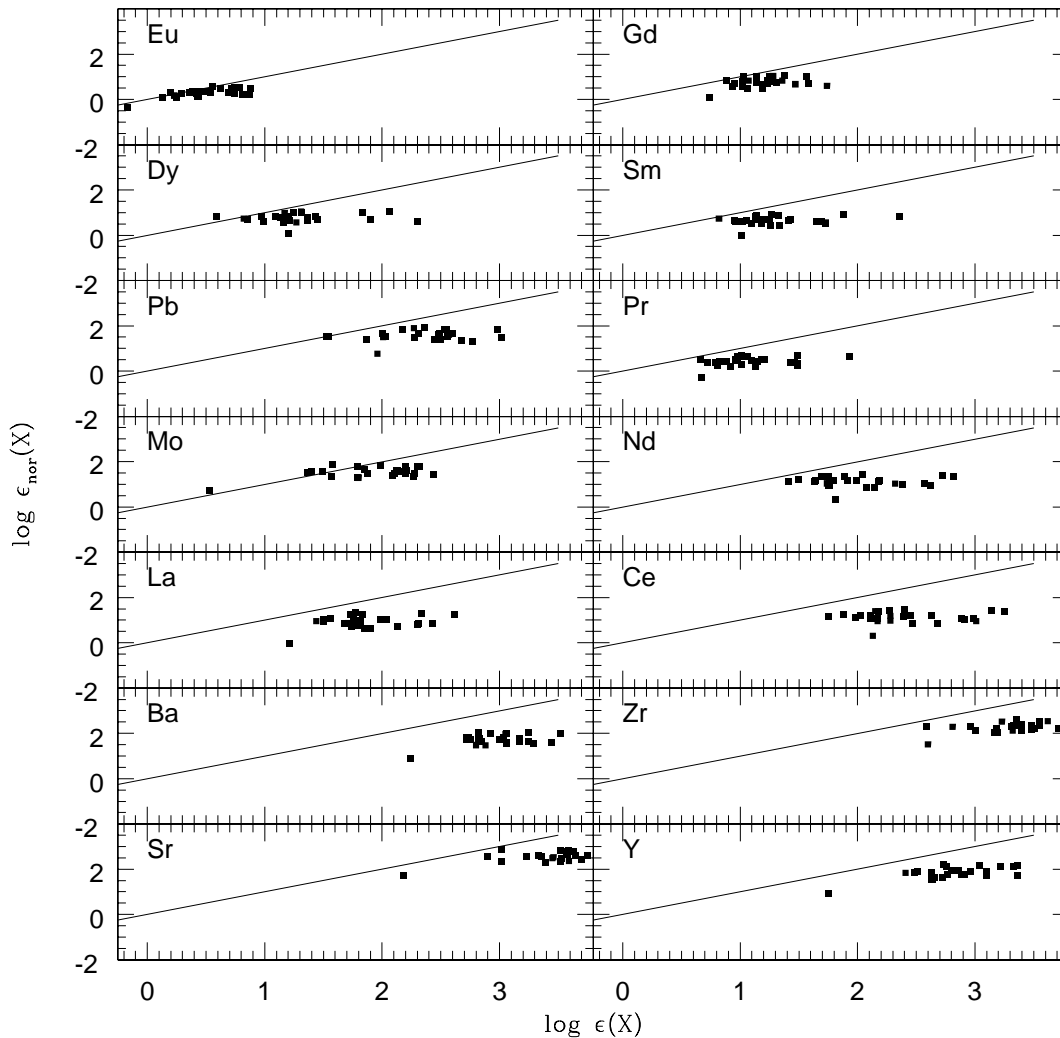


Fig. 3. Total abundances of heavy elements for the barium ($\log \epsilon(X)$) and normal ($\log \epsilon_{nor}(X)$) stars with the same metallicities. Solid lines indicate $\log \epsilon_{nor}(X) = \log \epsilon(X)$.

and $0.12 \leq [\text{Pr}/\text{Eu}] \leq 0.92$. There is no r-process contribution in the Pb abundance, according to Arlandini et al. (1999). 46% of contribution comes from s-process main component and 54% has been attributed in previous work to the strong s-process component. Data are in the ranges $-1.03 \leq [\text{Pb}/\text{Ba}] \leq 0.07$ and $-0.58 \leq [\text{Pb}/\text{Eu}] \leq 0.86$. Abundances of Pb obtained for barium stars are usually larger than those of Mo, which are larger than those of Pr, and the same is true for solar abundances. Only for 5 stars the Mo abundance is larger than those of Pb and for one star Pr abundance is larger than that of Mo. However, $[\text{X}/\text{Fe}]$ values are such that the values of $[\text{Mo}/\text{Ba}, \text{Eu}]$ are usually lower than $[\text{Pr}, \text{Pb}/\text{Ba}, \text{Eu}]$. As a consequence, the range for Mo involves lower values in Figure 11.

Elements formed mainly by the s-process main component can be divided into two groups: light s-elements around magic neutron number 50 and heavy s-elements around magic neutron number 82. In this work, Sr, Y, Zr were included in light s-elements and Ba, La, Ce, Nd in the heavy s-elements

groups. For these elements, s-process main component contribution is larger than 50% according to Arlandini et al. (1999). It is worth to emphasize that Sm is rather an r-element because its s-process contribution is less than 30% while r-process contributes with 67.4% of its production. The presence of light s-elements in very metal-poor stars cannot be entirely explained by an r-process contribution. For instance, there is no production of Sr by r-process, as shown in Table 4, and it is observed in the most metal-poor stars. Another nucleosynthetic process related to massive stars is needed in order to explain such observed abundances. Figure 9 from Burris et al. (2000) shows an increasing trend of $[\text{Sr}/\text{Ba}]$ toward lower metallicities $[\text{Fe}/\text{H}] < -1$. It has been suggested that beyond the observational uncertainties, another nucleosynthesis source would explain the increasing $[\text{Sr}/\text{Ba}]$ at lower metallicities, and this source could be the s-process weak component. According to Table 4, 14.9% of solar abundance of Sr come from the s-process weak component and 0.56% from the p-process. At metallicities as low

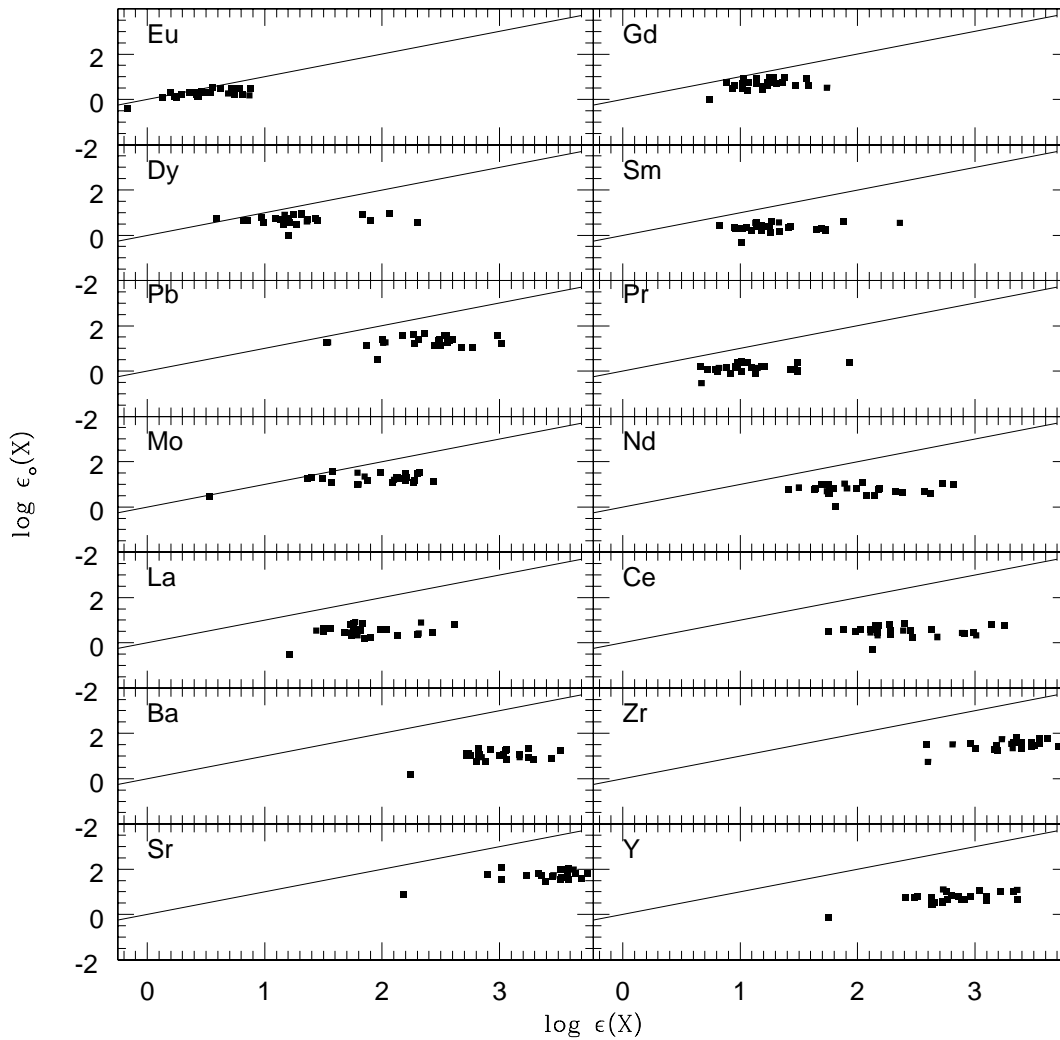


Fig. 4. Abundance fraction of heavy elements due to all processes except the s-process main component ($\log \epsilon_0(X)$) vs. total abundance of barium stars ($\log \epsilon(X)$). Solid lines indicate $\log \epsilon_0(X) = \log \epsilon(X)$

as $[\text{Fe}/\text{H}] < -3$, the Sr production is expected to be low, given that the s-process weak component is secondary and in such environment there is a lack of pre-existing seed nuclei.

Abundance ratios of light s-elements relative to Ba are shown in Table 7 and Figure 11. In the range of metallicities studied, the ratios are approximately constant in the ranges $-1 \leq [\text{Sr}/\text{Ba}] \leq 0.1$, $-0.75 \leq [\text{Y}/\text{Ba}] \leq 0.05$ and $-0.80 \leq [\text{Zr}/\text{Ba}] \leq 0.30$. AGB stars are included in the same range for $[\text{Zr}/\text{Ba}]$, while for $[\text{Y}/\text{Ba}]$ two of them show higher values, 0.25 and 0.66. Figure 9 from Burris et al. (2000) shows a dispersion around $[\text{Fe}/\text{H}] \approx -1$ with $-0.55 \leq [\text{Sr}/\text{Ba}] \leq 0.1$, similarly to the present sample barium stars.

5. Neutron Exposures

5.1. Theoretical predictions of Malaney (1987)

s-element nucleosynthesis depends on the neutron exposure to which the seed nuclei were submitted inside the AGB star.

Considering the scenario of material transfer for the barium star formation, it is reasonable to expect that the abundance patterns of barium stars show signatures of the neutron exposure during the occurrence of s-process in the AGB companion.

Models trying to reproduce the resulting abundances of s-process, were presented by Cowley & Downs (1980), who calculated theoretical abundances by using exact solutions from Clayton & Ward (1974) for models of exponential distribution, and the approximate solution from Clayton et al. (1961) for a model of single exposure.

Malaney (1987a) presented theoretical predictions of abundances from the s-process starting on iron seeds, considering single neutron exposure for several values of τ_0 and neutron density $n_n = 10^8 \text{ cm}^{-3}$. Malaney (1987b) also provides theoretical predictions, but considering an exponential neutron distribution for several values of τ_0 and two different values of neutron density, 10^8 cm^{-3} and 10^{12} cm^{-3} .

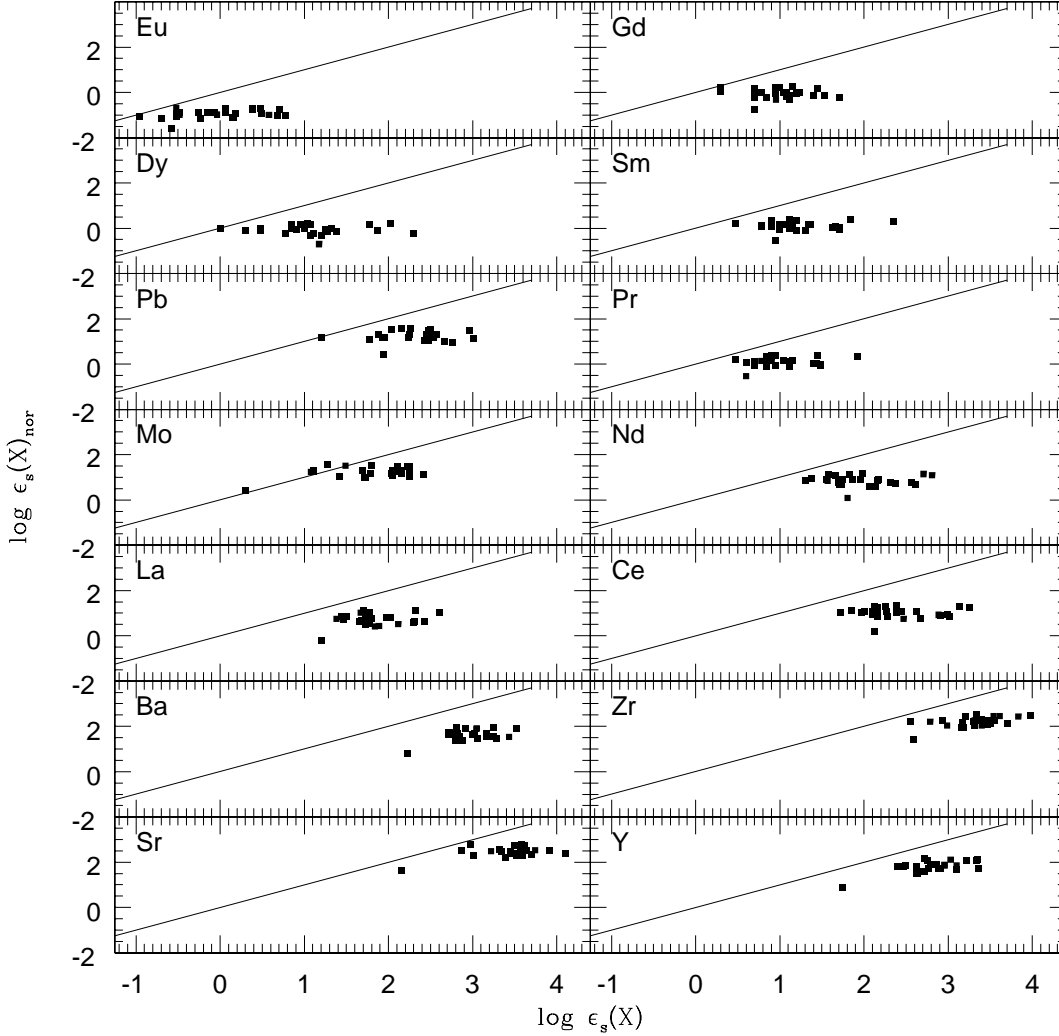


Fig. 5. Abundances corresponding to the s-process main component for heavy elements of barium stars ($\log \epsilon_s(X)$) vs. normal stars ($\log \epsilon_s(X)_{nor}$) with the same metallicities. Solid lines indicate $\log \epsilon_s(X)_{nor} = \log \epsilon_s(X)$.

Abundances resulting from theoretical predictions are usually normalized for $\log \epsilon_c(\text{Sr}) = 20$. Tomkin & Lambert (1983) provide an expression to transform observational data to this scale

$$\epsilon_c(X) = C(y - 1)\epsilon_o(X) \quad (15)$$

where y is the relative abundance between barium and normal stars of same metallicity

$$\log y = \log \epsilon(X) - \log \epsilon_{nor}(X)$$

where $\log \epsilon(X)$ of barium stars are those from Tables 13 and 14 of paper I and $\log \epsilon_{nor}(X)$ are those from Table 2. The value of C for each star is known by setting $\log \epsilon_c(\text{Sr}) = 20$.

In order to check the fit, Cowley & Downs (1980) used an expression largely used in the literature (e.g. van Winckel & Reyniers 2000; Pereira & Junqueira 2003).

$$S^2 = \frac{1}{N} \sum_{i=1}^N \frac{(O_i - P_i)^2}{\sigma_i^2} \quad (16)$$

where O_i are abundances $\log \epsilon_c(X)$ for each element “ i ”, P_i are theoretical predictions, N is the number of elements and σ is the uncertainty on $\log \epsilon_c(X)$ calculated by

$$\sigma_{\log \epsilon_c} = \sqrt{\sigma_{\log C}^2 + \frac{\sigma_{\log y}^2}{(1 - 10^{-\log y})^2} + \sigma_{\log \epsilon_o(X)}^2} \quad (17)$$

with

$$\sigma_{\log y} = \sqrt{\sigma_{\log \epsilon(X)}^2 + \sigma_{\log \epsilon_{nor}(X)}^2} \quad (18)$$

and the uncertainty on C

$$\sigma_{\log C} = \sqrt{\frac{\sigma_{\log y}^2}{(1 - 10^{-\log y})^2} + \sigma_{\log \epsilon_o(\text{Sr})}^2} \quad (19)$$

where y represents Sr, considering $\sigma_{\log \epsilon_c(\text{Sr})} = 0$.

The best fit between theoretical predictions and observational data correspond to the smallest value of S^2 . S^2 was calculated for all P values from Malaney (1987a) and Malaney

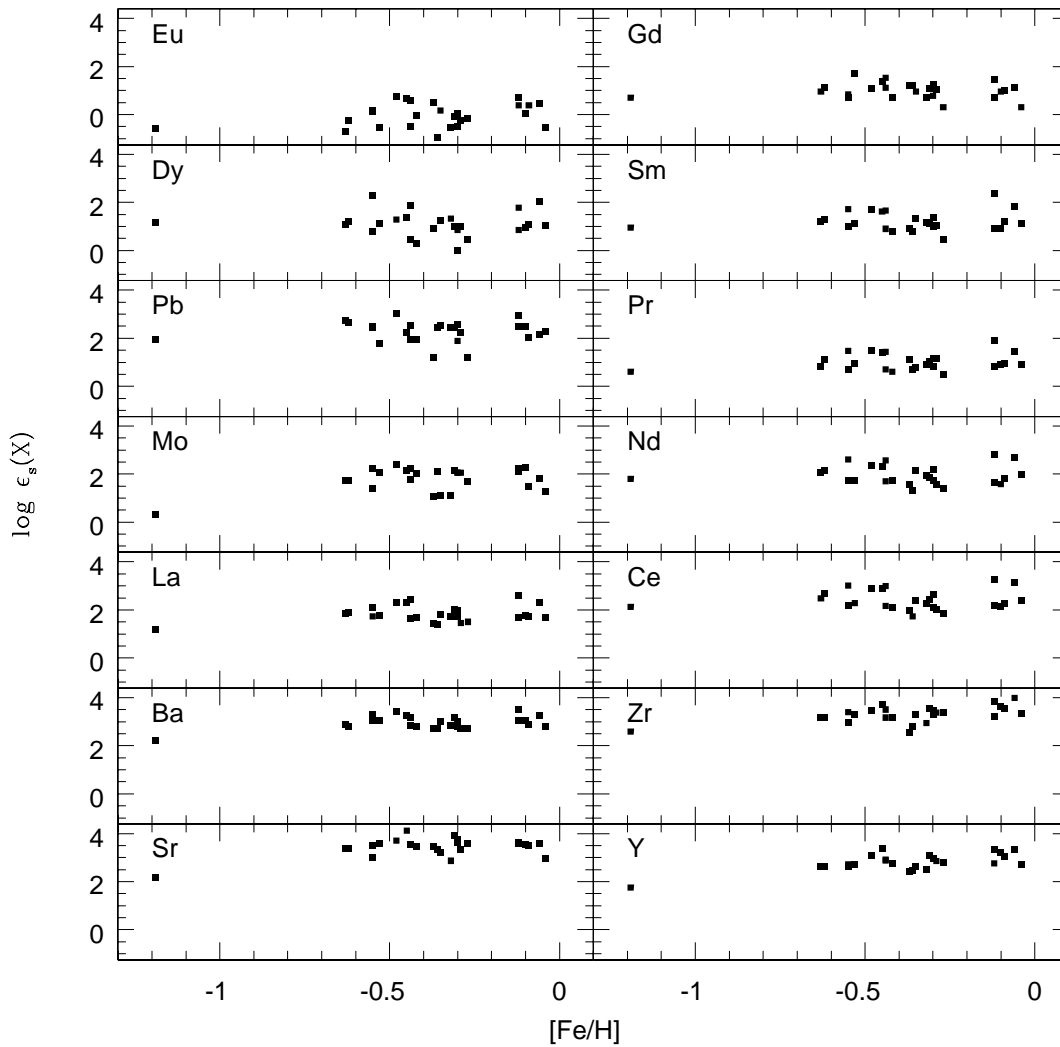


Fig. 6. $\log \epsilon_s(X)$ vs. $[\text{Fe}/\text{H}]$, where $\log \epsilon_s(X)$ are the abundances corresponding to the s-process main component of heavy elements in barium stars.

(1987b) tables. Table 8 shows the best fittings of S^2 and τ_o for each Malaney's table. Figures 12 to 15 show the best fittings obtained for each present sample barium star, showing the values of τ_o and neutron density n_n , in columns 8 and 9 of Table 8.

For some elements of some barium stars the differences between abundances of barium and normal stars were too small, although $\epsilon_{nor}(X) < \epsilon(X)$. It is the case of Mo (HD 749), Eu (HD 89948, HD 116869, HD 210709) and Gd (HD 22589). In these cases, the uncertainty on $\log \epsilon_c(X)$ is too large, decreasing the quality of the fit. They were withdrawn before using equation 16, and are easily seen in Figures 12 to 15 due their discrepant values with respect to theoretical predictions, and there are no error bars for them. Except for such cases, there is a good agreement between observed and theoretical data shown in Figures 12 to 15. For most stars, the best fit was that for which theoretical predictions consider an exponential neutron exposure distribution, with neutron density 10^{12} cm^{-3}

for 5 stars and 10^8 cm^{-3} for 14 stars. For 7 stars, the best fit was found for a single neutron exposure, and neutron density 10^8 cm^{-3} . This result is curious since the exponential neutron exposure distribution is more well accepted in the literature. However, Busso et al. (1999) suggested that s-process is a result of a number of single exposures instead of an exponential distribution. Pereira & Junqueira (2003) also obtained a single exposure and neutron density 10^8 cm^{-3} as the best fit for 2 barium stars. One of them, HD 87080, for which they found $\tau = 1.0$, is in common with the present sample, for which we found a best fit with an exponential distribution of $\tau = 0.6$ and neutron density 10^8 cm^{-3} . The reason of this difference is unclear. The metallicities adopted were very close (see Tables 9 and 11 from paper I), however, values of $\log \epsilon(X)$ in this work are usually higher than those from Pereira & Junqueira (2003). Least-squares fittings were used here to compute abundances of normal stars (equation 15), while Pereira & Junqueira (2003) used the sum of solar abundance with star metallicity as a reference.

Table 8. Results on neutron exposures. Columns 2 and 3 correspond to results of the fittings to theoretical predictions of Malaney (1987a) and columns 4 to 7, those of Malaney (1987b). $S^2(u)$, $S^2(e8)$, $S^2(e12)$ are the fit quality, respectively, for single exposure, exponential exposure under neutron density 10^8 cm^{-3} and exponential exposure under neutron density 10^{12} cm^{-3} . τ_o^a , τ_o^b and τ_o^c are the mean distributions of neutron exposure corresponding to $S^2(u)$, $S^2(e8)$ and $S^2(e12)$, respectively. $\tau_o(f)$ and n_n are results corresponding to smaller S^2 . Column 10 shows if the best fit corresponds to exponential (exp) or single (sing) exposure. Columns 11 to 13 correspond to results of fit of σN curves, being χ_{red} the quality of the fit. Numbers in parenthesis are errors in last decimals, and were estimated directly from the fittings. The uncertainties on τ_o^a , τ_o^b and τ_o^c were estimated in 0.1 mb^{-1} . For all cases, τ_o is given in mb^{-1} . Number in parenthesis are errors in last decimals.

star	$S^2(u)$	τ_o^a	$S^2(e8)$	τ_o^b	$S^2(e12)$	τ_o^c	$\tau_o(f)$	n_n	exp	$\tau_o(\sigma N)$	G(%)	χ_{red}
HD 749	0.69	1.00	0.52	0.80	0.77	0.80	0.8	10^8	exp	0.406(5)	0.568(19)	0.73
HR 107	0.98	0.10	1.47	0.20	1.30	0.30	0.1	10^8	sing	0.43(6)	0.083(20)	0.56
HD 5424	0.85	1.10	1.15	0.80	1.71	0.80	1.1	10^8	sing	1.05(1)	0.086(1)	0.94
HD 8270	1.33	0.90	1.21	0.20	1.46	0.30	0.2	10^8	exp	0.27(1)	0.35(3)	0.41
HD 12392	0.46	1.10	0.38	0.80	0.79	0.80	0.8	10^8	exp	0.40(2)	0.73(3)	0.59
HD 13551	1.57	0.90	1.25	0.20	1.44	0.30	0.2	10^8	exp	0.22(1)	1.06(56)	0.50
HD 22589	1.10	0.80	0.89	0.20	1.27	0.20	0.2	10^8	exp	0.187(23)	1.25(54)	0.52
HD 27271	0.26	0.90	0.24	0.40	0.16	0.05	0.05	10^{12}	exp	0.272(14)	0.568(19)	0.35
HD 48565	3.14	1.00	1.34	0.40	2.66	0.05	0.4	10^8	exp	0.659(10)	0.0631(23)	0.32
HD 76225	0.80	0.10	0.71	0.20	1.83	0.30	0.2	10^8	exp	0.25(1)	0.83(12)	0.38
HD 87080	2.22	1.00	1.17	0.60	2.49	0.80	0.6	10^8	exp	0.71(1)	0.145(5)	0.48
HD 89948	0.67	0.10	0.45	0.20	1.65	0.30	0.2	10^8	exp	0.24(2)	0.77(36)	0.30
HD 92545	1.42	0.90	1.22	0.20	0.85	0.30	0.3	10^{12}	exp	0.291(3)	0.261(14)	0.40
HD 106191	1.36	0.90	1.16	0.40	0.72	0.05	0.05	10^{12}	exp	0.383(1)	0.130(1)	0.38
HD 107574	1.91	0.90	2.28	0.20	2.05	0.30	0.9	10^8	sing	0.298(2)	0.245(5)	0.42
HD 116869	0.14	1.10	0.18	0.80	0.33	0.80	1.1	10^8	sing	0.55(2)	0.0646(22)	0.55
HD 123396	0.46	1.10	0.84	0.80	1.24	0.80	1.1	10^8	sing	0.54(2)	0.0315(22)	0.54
HD 123585	2.17	1.00	0.98	0.40	2.14	0.50	0.4	10^8	exp	0.46(1)	0.275(15)	0.46
HD 147609	2.33	0.10	1.90	0.20	2.42	0.30	0.2	10^8	exp	0.288(7)	1.07(11)	0.41
HD 150862	0.66	0.90	1.57	0.20	1.11	0.30	0.9	10^8	sing	0.271(3)	0.489(26)	0.47
HD 188985	1.83	0.90	1.77	0.40	1.94	0.40	0.4	10^8	exp	0.401(4)	0.225(5)	0.39
HD 210709	0.11	1.10	0.19	0.80	0.26	0.80	1.1	10^8	sing	0.314(3)	0.303(9)	0.38
HD 210910	0.55	0.10	0.63	0.20	0.38	0.30	0.3	10^{12}	exp	0.44(4)	0.075(13)	0.52
HD 222349	3.02	0.90	1.28	0.40	2.00	0.05	0.4	10^8	exp	0.379(8)	0.170(12)	0.46
BD+18 5215	2.41	0.90	2.74	0.40	1.50	0.05	0.05	10^{12}	exp	0.274(1)	0.503(2)	0.63
HD 223938	0.26	1.00	0.20	0.50	0.29	0.70	0.5	10^8	exp	0.384(5)	0.229(9)	0.34

5.2. σN Curve

Another way to evaluate the neutron exposure nature is through σN curves. For such, the cross section values (σ_c (30keV), column 13 of Table 4) and abundances related to the s-process main component of each nuclide (from equation 9) are needed. Results of σN curve for each barium star are shown in column 11 of Table 6.

The uncertainty on σN is given by the expression

$$\sigma_{\sigma N} = \sigma_c \epsilon_s(X) \sqrt{\left(\frac{\sigma_{\epsilon_s}}{\epsilon_s}\right)^2 + \left(\frac{\sigma_{\sigma_c}}{\sigma_c}\right)^2}. \quad (20)$$

In the literature, σN is found in Si scale, where $\epsilon(\text{Si}) = 10^6$. Anders & Grevesse (1989) provide the following relation between the Si scale and the scale where $\log \epsilon(X) = \log(n_x/n_H) + 12$:

$$\epsilon(X)_{Si} = 10^{\log \epsilon(X) - x} \quad (21)$$

where $x = 1.554 \pm 0.020$, and the uncertainty is

$$\sigma_{\epsilon Si} = \epsilon(X)_{Si} \sqrt{(\ln 10 \sigma_{\log \epsilon Si})^2 + \sigma_x^2}. \quad (22)$$

To compute abundances relative to the s-process main component in the Si scale it is necessary to transform abundances of normal stars to this scale. Then the distribution relative to each process in the Si scale is done in the same way to usual scales. Column 16 of Table 6 shows the results of $\sigma N = \sigma_c \epsilon_s(X)_{Si}$ for nuclides of barium stars.

For comparison purposes, the distribution of abundance in several nucleosynthetic processes were also done. The total abundance of an element of a barium star was distributed in solar proportions, with fractions corresponding to s-, r- and p-processes, shown in columns 3 to 7 in Table 4. Results for this σN curve are shown in column 18 of Table 6, and they are represented by open symbols in Figures 18 to 21. These results are lower than others because the overabundance derived from the s-process is neglected.

A theoretical σN curve is calculated with equation 1, where two parameters (τ_o and G) must be determined by fitting observed data. A robust statistics was used, which, in this work, consists in finding values of G and τ_o that simultaneously minimize the sum of absolute deviations represented by

$$\chi = \sum |f(x_k) - y_k|,$$

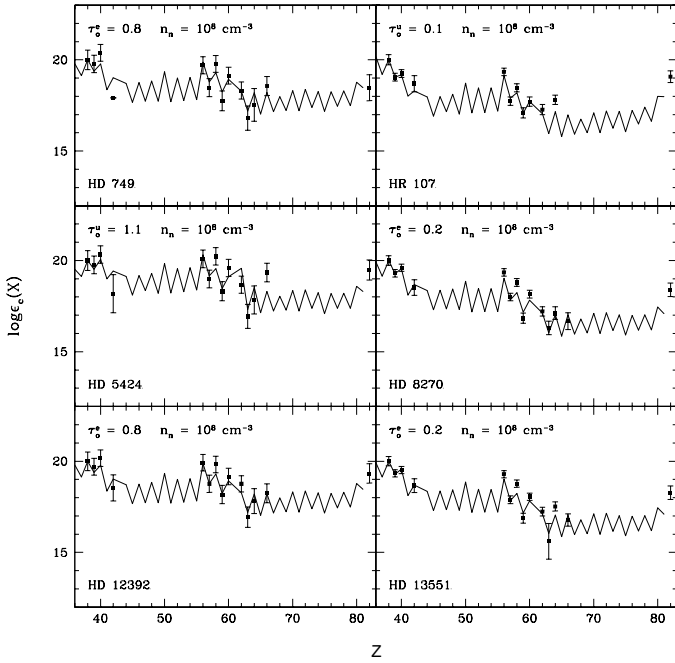


Fig. 12. Fittings of observed data to theoretical predictions by Malaney (1987a,b).

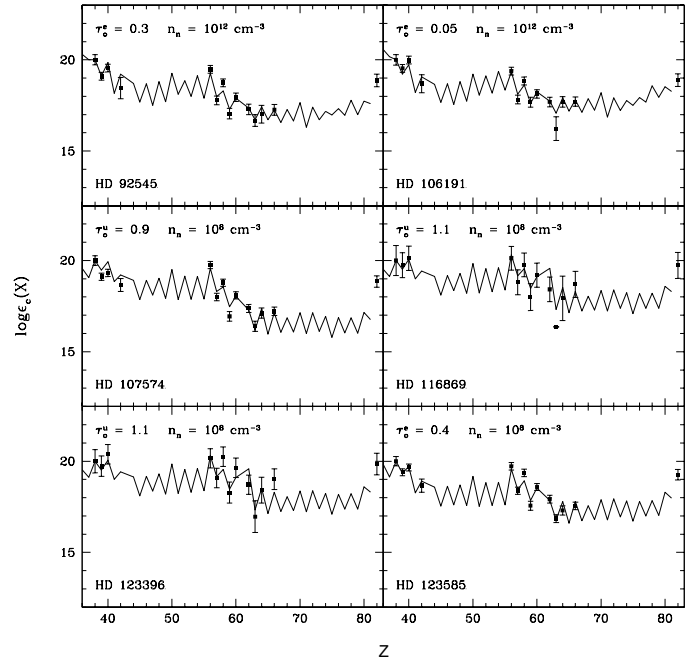


Fig. 14. Same as Figure 12 for other 6 sample stars.

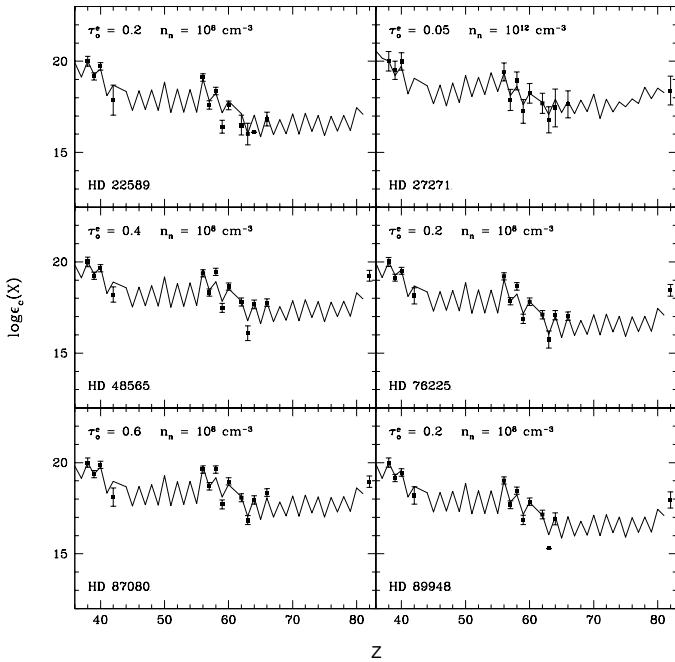


Fig. 13. Same as Figure 12 for other 6 sample stars.

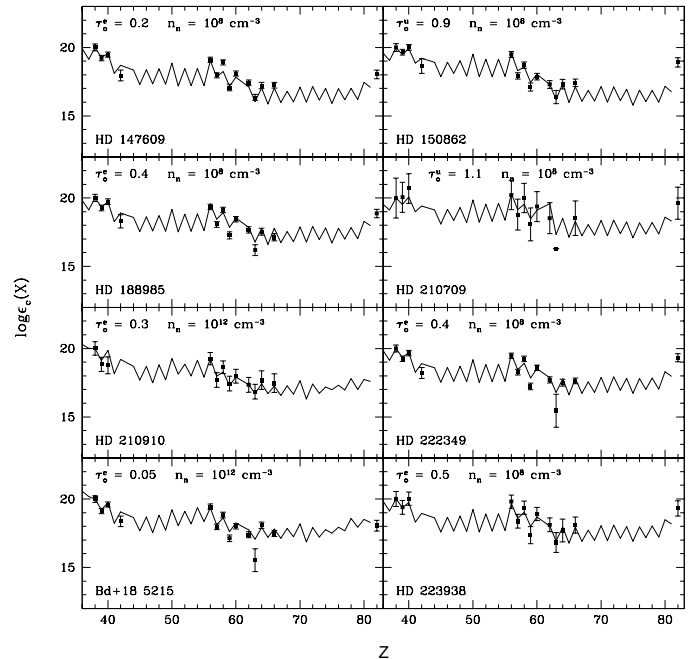


Fig. 15. Same as Figure 12 for other 8 sample stars.

where $f(x_k)$ is the theoretical value calculated with equation 1 and y_k is the value calculated directly for σN by using observed data. Data very far from the curve were neglected. Figure 16 shows the functions that minimize χ relative to each parameter. The crossing point of these functions provides the values of G and τ_o that minimize simultaneously both functions. More

details on this procedure are found in Allen & Horvath (2000). Table 8 shows results of the fittings and their $\chi_{red} = \chi/(n-2)$, where n is the number of data, representing the goodness of fits.

The method was tested for the Sun, by using data from Arlandini et al. (1999). The resulting line from the fitting is shown in Figure 17, in which $\tau_o = 0.345 \pm 0.005 \text{ mb}^{-1}$ and

$G = 0.043 \pm 0.002\%$. Figure 19b from Käppeler et al. (1989) shows their solar σN curve, resulting $\tau_o = 0.30 \pm 0.01 \text{ mb}^{-1}$ and $G = 0.043 \pm 0.002\%$. Figures 18 to 21 show that the uncertainties, represented by error bars, are very large for barium stars, and for this reason they were neglected in computing the quality of the fit. Branching and too discrepant data were also neglected.

For the present sample, theoretical σN curves fit very well the observed data, as shown in Figures 18 to 21. This confirms that the solar isotopic composition is adequate for barium stars, and that the transfer of enriched material keeps approximately the solar proportions of each nuclide. In order to build the theoretical curve, one considers that at the beginning of the neutron capture chain, abundances of all elements heavier than iron are null. This supposition gets more distant from the truth as the metallicity increases. Furthermore, the fit brings some difficulties: a) there is a lack of elements along the curve due to the difficulty in finding lines in the spectrum, preventing a higher quality of the fit between theoretical and observed curves; b) barium stars data show a large dispersion; c) branching values were not considered; d) numerical solution of equation 1 is difficult, given that two parameters to be fitted appear in non linear form in the equation. The good agreement between theoretical and observed curves is interesting, taking into account all assumptions and difficulties found in their building.

5.3. s-process indices

One way to relate light and heavy s-elements is through hs and ls indices, defined as the mean of abundances of light and heavy elements, respectively. According to section 4.3, Sr, Y and Zr were included into ls, and Ba, La, Ce and Nd were included into hs. For the s index, all these heavy and light s-elements were considered. $[\text{hs}/\text{ls}] = [\text{hs}/\text{Fe}] - [\text{ls}/\text{Fe}]$ was also computed. In the case of missing abundances, such element was excluded from the index. Figure 22 and Table 9 show $[\text{hs}/\text{ls}]$, $[\text{ls}/\text{Fe}]$, $[\text{hs}/\text{Fe}]$ and $[\text{s}/\text{Fe}]$ vs. $[\text{Fe}/\text{H}]$. Uncertainties on $[\text{s}/\text{Fe}]$, $[\text{ls}/\text{Fe}]$ and $[\text{hs}/\text{Fe}]$ have to take into account the contribution of the uncertainties on abundances of each element included in the index.

A behaviour of $[\text{hs}/\text{ls}]$ as a function of τ_o can be inferred from the slope of the σN curve. The larger τ_o , the smaller is the slope, and, at the same time, a smaller slope means larger abundance of heavy s-elements located on the right end of the curve. The conclusion is that the larger τ_o , the larger also is $[\text{hs}/\text{ls}]$, as shown in Figure 17 of Wallerstein et al. (1997). It is reasonable considering that the chain of formation of s-elements cannot go far if the neutron flux is low.

During the third dredge-up, an amount of protons is introduced in the intershell, a region composed of helium located between helium and hydrogen burning shells. These protons are captured by ^{12}C and form ^{13}C through the reaction $^{12}\text{C}(p,\gamma)^{13}\text{N}(\beta^+\nu)^{13}\text{C}$ or ^{14}N through $^{13}\text{C}(p,\gamma)^{14}\text{N}$, creating the ^{13}C pocket. If the thermal pulse is independent of metallicity, protons are introduced in the intershell in the same amounts for higher or lower metallicities. It means that the neutron source $^{13}\text{C}(\alpha,n)^{16}\text{O}$, likely the main neutron source in AGB stars, is in-

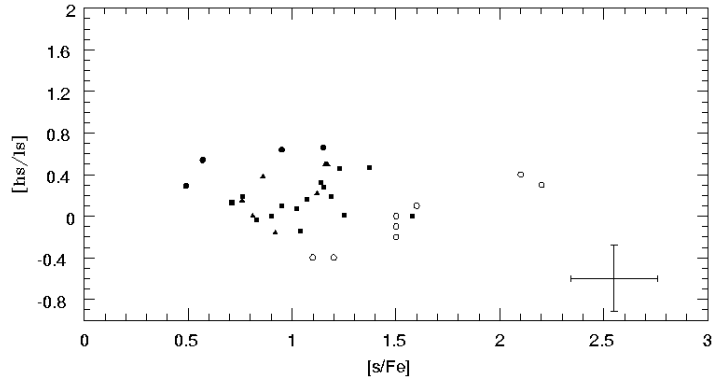


Fig. 23. $[\text{hs}/\text{ls}]$ vs. $[\text{s}/\text{Fe}]$. Symbols are the same as in Figure 7. Error bars in bottom right showing the largest uncertainties.

dependent of metallicity. However the neutron number by seed iron nucleus will be larger at low metallicities (Clayton 1988). If τ_o is proportional to $[\text{hs}/\text{ls}]$ and inversely proportional to $[\text{Fe}/\text{H}]$, $[\text{hs}/\text{ls}]$ will be also inversely proportional to $[\text{Fe}/\text{H}]$, so it is expected that the lower the metallicity, the larger the ratio $[\text{hs}/\text{ls}]$. Figure 24 confirms a correlation between τ_o and $[\text{hs}/\text{ls}]$ for barium and post-AGB stars. However, the anticorrelation between $[\text{hs}/\text{ls}]$ and $[\text{Fe}/\text{H}]$ is weak for barium and post AGBs stars, as shown in Figure 22. In the same way, the anticorrelation between τ_o and $[\text{Fe}/\text{H}]$ is not confirmed in Figure 24. The yield of all s-elements to decrease with decreasing metallicities is compatible with the secondary characteristic of s-process, which requires pre-existing seed nuclei. At intermediate metallicities (≈ -0.8) the Ba peak is dominant among s-process products in AGB models (Busso et al. 1999). For higher metallicities the Zr peak dominates. If giant as well as dwarf barium stars have the same physical origin for the accretion of enriched material from a more evolved companion, it is reasonable to expect that if the neutron exposure is higher for dwarf more metal deficient stars, the same occurs for giants.

In Figure 24, τ_o derived from the σN curve are mainly within $1.8 < \tau_o < 0.6$, with less spread as compared to those derived from theoretical predictions by Malaney (1987a,b), however both show the same trend. For giant stars $\tau_o \approx 1$ was found from theoretical predictions, but not from the σN curves.

Solid and dashed lines in Figure 24 are least-squares fittings, with parameters:

$$[\text{hs}/\text{ls}] = (0.423 \pm 0.095)\tau_o + (0.011 \pm 0.043) \quad (23)$$

$$[\text{hs}/\text{ls}] = (0.899 \pm 0.173)\tau_o + (-0.160 \pm 0.068) \quad (24)$$

where equation 23 uses τ_o values from theoretical predictions by Malaney (1987a,b), with $\chi^2_{\text{red}} = 1.710$ and equation 24 uses τ_o values derived from σN curves, with $\chi^2_{\text{red}} = 1.464$. Regarding χ^2_{red} , in both cases the linear and increasing correlation toward higher values of τ_o have good quality.

Figure 10 from van Winckel & Reyniers (2000) shows $[\text{hs}/\text{ls}]$ vs. $[\text{Fe}/\text{H}]$ including data from several previous work. Despite the dispersion, $[\text{hs}/\text{ls}]$ increases toward higher $[\text{Fe}/\text{H}]$. The dependence of neutron exposure on $[\text{Fe}/\text{H}]$ could indicate that other important parameters affect dredge-up events and nucleosynthetic processes along the red giant branch evolution.

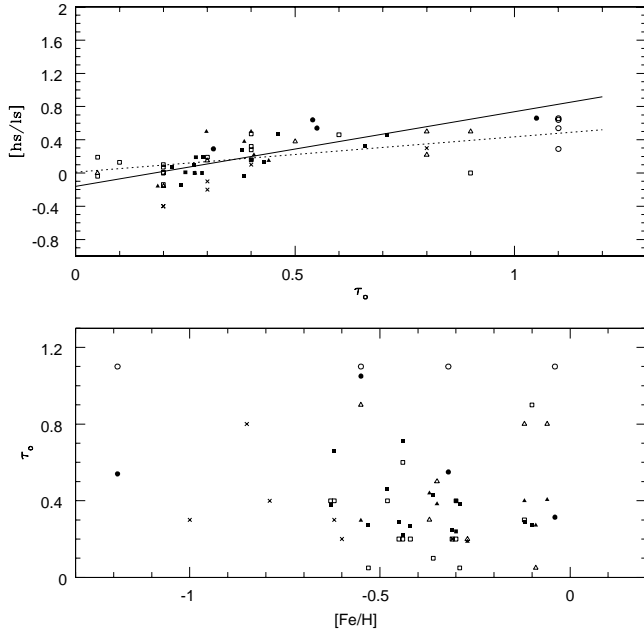


Fig. 24. $[hs/ls]$ vs. τ_o (upper panel), and τ_o vs. $[Fe/H]$ (lower panel). Crosses are post-AGBs from Reyniers et al. (2004) and van Winckel & Reyniers (2000). Circles, triangles and squares represent the sample barium stars according to $\log g$, as in Figure 7. Open symbols correspond to τ_o values derived from theoretical predictions by Malaney (1987a,b) and filled symbols are those from σN curves. Solid line is the least-squares fitting with τ_o from σN curves and dotted, with τ_o from theoretical predictions.

For the present sample barium stars, $[s,ls,hs/Fe]$ and $[hs/ls]$ slightly decrease toward higher metallicities, in the range $0.45 \leq [s/Fe] \leq 1.6$, $0.4 \leq [ls/Fe] \leq 1.6$, $0.7 \leq [hs/Fe] \leq 1.75$ and $-0.2 \leq [hs/ls] \leq 0.7$. According to Wheeler et al. (1989), $[s/Fe] = 0$ for less evolved stars in this same range of metallicities, therefore, the results found for the present sample show the overabundance of s-elements in barium stars.

One has to be careful in comparing the indices of the present work to those of post-AGBs in Figures 11, 23 and 22, given that Reyniers et al. (2004) and van Winckel & Reyniers (2000) included Sm and not Ce in s and hs, and only Y and Zr in ls. Figure 23 shows that $[hs/ls]$ vs. $[s/Fe]$ has a large dispersion for barium stars whereas for post-AGBs there is a linear correlation. Figure 8 from Reyniers et al. shows the same correlation but using different combinations of the elements included in the indices. One of them uses Ce, however, the linear correlation is still present comparing with using Ba, La, Nd and Sm in hs. Other configurations show larger dispersion, hence the presence of Ce in hs and s is not the origin of the dispersion for barium stars.

According to Table 7 and Figure 11, there is no difference as a function of $\log g$, confirming that the overabundances characteristic of a barium star do not depend on luminosity classes.

Table 9. s-process indices: s, ls and hs for present sample barium stars.

star	[s/Fe]	[ls/Fe]	[hs/Fe]	[hs/ls]
HD 749	1.12±0.21	1.09±0.23	1.31±0.22	0.22±0.32
HR 107	0.71±0.08	0.69±0.09	0.82±0.07	0.13±0.11
HD 5424	1.15±0.21	0.98±0.23	1.64±0.22	0.66±0.32
HD 8270	0.95±0.08	0.93±0.09	1.03±0.07	0.10±0.11
HD 12392	1.17±0.21	1.07±0.23	1.57±0.22	0.50±0.32
HD 13551	1.02±0.08	1.02±0.09	1.08±0.07	0.07±0.11
HD 22589	0.92±0.08	0.93±0.09	0.77±0.07	-0.16±0.11
HD 27271	0.81±0.21	0.81±0.23	0.81±0.22	0.00±0.32
HD 48565	1.14±0.08	1.08±0.09	1.40±0.07	0.32±0.11
HD 76225	1.25±0.08	1.25±0.09	1.26±0.07	0.01±0.11
HD 87080	1.23±0.08	1.13±0.09	1.59±0.07	0.46±0.11
HD 89948	1.04±0.08	1.06±0.09	0.92±0.07	-0.14±0.11
HD 92545	0.76±0.08	0.73±0.09	0.92±0.07	0.19±0.11
HD 106191	0.83±0.08	0.83±0.09	0.80±0.07	-0.04±0.11
HD 107574	1.16±0.08	1.05±0.09	1.55±0.07	0.50±0.11
HD 116869	0.57±0.21	0.45±0.23	0.99±0.22	0.54±0.32
HD 123396	0.95±0.21	0.79±0.23	1.44±0.22	0.64±0.32
HD 123585	1.37±0.08	1.27±0.09	1.74±0.07	0.47±0.11
HD 147609	1.58±0.08	1.58±0.09	1.58±0.07	0.00±0.11
HD 150862	0.90±0.08	0.90±0.09	0.91±0.07	0.00±0.11
HD 188985	1.07±0.08	1.05±0.09	1.20±0.07	0.16±0.11
HD 210709	0.49±0.21	0.44±0.23	0.73±0.22	0.29±0.32
HD 210910	0.76±0.21	0.74±0.23	0.89±0.22	0.15±0.32
HD 222349	1.15±0.08	1.10±0.09	1.38±0.07	0.28±0.11
BD+18 5215	1.19±0.08	1.17±0.09	1.35±0.07	0.19±0.11
HD 223938	0.86±0.21	0.79±0.23	1.17±0.22	0.38±0.32

Table 10. s-process indices s, ls and hs for barium stars collected in the literature. References: N94 - North et al. (1994); LB91 - Luck & Bond (1991).

star	[Fe/H]	[ls/Fe]	[hs/Fe]	[hs/ls]	ref
48565	-0.90	0.70	1.07	0.37	N94
76225	-0.50	1.13	1.11	-0.02	N94
89948	-0.13	1.20	0.70	-0.50	LB91
92545	-0.33	0.49	0.68	0.19	N94
106191	-0.40	0.86	0.59	-0.27	N94
107574	-0.80	0.85	1.22	0.37	N94
123585	-0.50	1.28	1.50	0.22	N94
123585	-0.50	1.10	1.10	0.00	LB91
147609	-0.50	0.88	0.98	0.10	N94
150862	-0.30	1.05	0.61	-0.44	N94
150862	-0.20	0.60	0.40	-0.20	LB91
188985	-0.30	1.02	1.10	0.08	N94

6. Conclusions

In this work, s-, r- and p-processes in barium stars were studied relative to normal stars.

Abundances of elements with lower contribution from the s-process main component are closer to the normal stars, whereas elements with higher s-contribution are more overabundant. However, r-elements such as Sm, Eu Gd and Dy are also enriched in barium stars sometimes at similar magnitudes as s-elements, and this occurs because the s-process main component chain includes the r-elements with $A < 209$.

The ratios involving light s-elements (Sr, Y and Zr) and Ba, a heavy s-element, are approximately constant in the range of metallicities of the present sample, with a dispersion similar to normal stars and post-AGBs.

Considering that the abundance fraction due to all processes except the s-process main component was present in the proto-barium star, it was possible to isolate the fraction corresponding to the s-process main component for barium stars. The solar isotopic distribution of this abundance fraction was used to build observed σ N curves. Their fittings to theoretical curves indicate that it is possible to use solar isotopic mix to estimate the contribution of the s-process main component for each isotope of an element.

The derivation of τ_o was obtained by fitting observed data to theoretical predictions and σ N curves. Theoretical predictions for abundances starting with Sr fit very well the observed data for the present sample, providing an estimation for neutron exposure occurred in AGB supplying s-process. The [hs/lr] vs. τ_o considering these theoretical predictions linearly increases, whereas for τ_o vs. [Fe/H] no conclusion was reached. The τ_o values from σ N fittings also provide linear and increasing τ_o vs. [hs/lr], but in this case, data are in the range $0.2 \leq \tau_o \leq 0.8$, showing lower dispersion than those for theoretical predictions.

Abundances obtained for barium stars are close to those for AGBs stars, but they are usually lower. This is reasonable considering that only part of the surface material of AGBs is transferred to the companion, that becomes a barium star.

Acknowledgements. We acknowledge partial financial support from the Brazilian Agencies CNPq and FAPESP. DMA acknowledges a FAPESP PhD fellowship n° 00/10405-8 and a FAPERJ post-doctoral fellowship n° 152.680/2004. We are grateful to Marcelo Porto Allen for making available his robust statistics code, and to the referee, Nils Ryde, for useful comments.

References

- Alpher, R.A., Bethe, H., Gamow, G. 1948, *PhRv*, 74, 505
- Allen, D.M., Barbuy, B. 2006, submitted (paper I)
- Allen, M.P., Horvath, J.E. 2000, *MNRAS*, 317, 23
- Anders, E.H., Grevesse, N. 1989, *Geochim.Cosmochim.Acta*, 53, 197
- Argast, D., Samland, M., Thielemann, F.-K., Qian, Y.-Z. 2004, *A&A*, 416, 997
- Arlandini, C., Käppeler, F., Wisshak, K., 1999 *ApJ*, 525, 886
- Arnould, M. 1976, *A&A*, 46, 117
- Arnould, M., Paulus, G., Jorissen, A. 1992, *A&A*, 254, 9L
- Bao, Z.Y., Beer, H., Käppeler, F., Voss, F., Wisshak, K. 2000, *At.Data.Ncl.Tabs.*, 76, 70
- Barbuy, B., Perrin, M.-N., Katz, D., Coelho, P., Cayrel, R., Spite, M., Van't Veer-Menneret, C. 2003, *A&A*, 404, 661
- Burbidge, E.M., Burbidge, G.R., Fowler, W.A., Hoyle, F. 1957, *Rev. Mod. Phys.*, 29, 547
- Burris, D.L., Pilachowski, C.A., Armandroff, T.E., Sneden, C., Cowan, J.J., Roe, H. 2000, *ApJ*, 544, 302
- Busso, M., Gallino, R., Wasserburg, G.J. 1999, *ARA&A*, 37, 239
- Cayrel, R., Perrin, M.N., Barbuy, B., Buser, R. 1991, *A&A*, 247, 108
- Clayton, D.D. 1988, *MNRAS*, 234, 1
- Clayton, D.D., Fowler, W.A., Hull, T.E., Zimmerman, B.A. 1961, *Ann.Phys.*, 12, 331
- Clayton, D.D., Ward, R.A. 1974, *ApJ*, 193, 397
- Cowan, J.J., Sneden, C., Burles, S., et al., 2002 *ApJ*, 572, 861
- Cowley, C.R., Downs, P.L. 1980, *ApJ*, 236, 648
- Edvardsson, B., Andersen, J., Gustafsson, B., Lambert, D.L., Nissen, P.E., Tomkin, J. 1993, *A&A*, 275, 101
- Freiburghaus, C., Rosswog, S., Thielemann, F.-K. 1999, *ApJ*, 525, L121
- Goriely, S., García-Senz, D., Bravo, E., José, J. 2005, *A&A*, 444, L1
- Gratton, R.G., Sneden, C. 1994, *A&A*, 287, 927
- Hill, V., Plez, B., Cayrel, R., et al. 2002, *A&A*, 387, 560
- Honda, S., Aoki, W., Kajino, T., Ando, H., Beers, T.B., Izumura, H., Sadakane, K., Takada-Hidai, M. 2004, *ApJ*, 607, 474
- Hoyle, F. 1946, *MNRAS*, 106, 343
- Ishimaru, Y., Wanajo, S., Aoki, W., Ryan, S.G. 2004, *ApJ*, 600, L47
- Jehin, E., Magain, P., Neuforge, C., Noels, A., Parmentier, G., Thoul, A.A. 1999, *A&A*, 341, 241
- Junqueira, S., Pereira, C.B. 2001, *AJ*, 122, 360
- Käppeler, F., Beer, H., Wisshak, K. 1989, *Rep.Prog.Phys.*, 52, 945
- Kaufer, A., Stahl, O., Tubbesing, S., et al. 2000, *Proc. SPIE*, 1008, 459
- Lamb, S.A., Howard, W.M., Truran, J.W., Iben, I.Jr. 1977, *ApJ*, 217, 213
- Luck, R.E., Bond, H.E. 1991, *ApJS*, 77, 515
- Lugaro, M., Davis, A.M., Gallino, R., Pellin, M.J., Straniero, O., Käppeler, F. 2003, *ApJ*, 593, 486
- Malaney, R.A. 1987a, *ApJ*, 321, 832
- Malaney, R.A. 1987b, *ApJS*, 137, 251
- Mashonkina, L., Gehren, T. 2001, *A&A*, 376, 232
- Mashonkina, L., Gehren, T., Travaglio, C., Borkova, R. 2003, *A&A*, 397, 275
- Meyer, B.S. 1994, *ARA&A*, 32, 153
- North, P., Berthet, S., Lanz, T. 1994, *A&A*, 281, 775
- O'Brien, S., Dababneh, S., Heil, M., Käppeler, F., Plag, R., Reifarh, R., Gallino, R., Pignatari, M. 2003, *Phys.Rev.C*, 68, 35801
- Pereira, C.B., Junqueira, S. 2003, *A&A*, 402, 1061
- Plez, B., Brett, J.M., Nordlund, A. 1992, *A&A*, 256, 551
- Qian, Y.-Z. 2000, *ApJ*, 534, L67
- Qian, Y.-Z. 2001, *ApJ*, 552, L117
- Raiteri, C.M., Gallino, R., Busso, M., Neuberger, D., Käppeler, F. 1993, *ApJ*, 419, 207
- Rayet, M., Arnould, M., Hashimoto, M., Prantzos, N., Nomoto, K. 1995, *A&A*, 298, 517
- Rayet, M., El Eid, M., Arnould, M. 1993, Käppeler, F., Wisshak, K. (eds.) *Nuclei in the Cosmos*. Institute of Physics Publishing, Bristol p. 613
- Reyniers, M., van Winckel, H., Gallino, R., Straniero, O. 2004, *A&A*, 417, 269
- Rosswog, S., Davies, M.B., Thielemann, F.-K., Piran, T. 2000, *A&A*, 360, 171
- Rosswog, S., Liebendörfer, M., Thielemann, F.-K., et al. 1999, *A&A*, 341, 499
- Smith, V.V., Suntzeff, N.B., Cunha, K., Gallino, R., Busso, M., Lambert, D.L. Straniero, O. 2000, *AJ*, 119, 1239
- Sneden, C., Cowan, J.J., Lawler, J.E., et al. 2003, *ApJ*, 591, 936

- Sneden, C., McWilliam, A., Preston, G.W., et al. 1996, *ApJ*, 467, 819
- Spite, M. 1967, *Ann.. Astrophys.* 30, 211
- Travaglio, C., Galli, D., Gallino, R., et al. 1999, *ApJ*, 521, 691
- Tomkin, J., Lambert, D.L. 1983, *ApJ*, 273, 722
- Tomkin, J., Lambert, D.L. 1999, *ApJ*, 523, 234
- Truran, J.W., Cowan, J.J., Pilachowski, C.A., Sneden, C. 2002, *PASP*, 114, 1293
- van Winckel, H., Reyniers, M. 2000, *A&A*, 354, 135
- Wallerstein, G., Iben, Jr.I., Parker, P., Boesgaard, A.M., Hale, G.M., Champagne, A.E., Barnes, C.A., Käppeler, F., Smith, V.V., Hoffman, R.D., Timmes, F.X. Sneden, C., Boyd, R.N., Meyer, B.S., Lambert, D.L. 1997, *Rev.Mod.Phys.*, 69, 995
- Wanajo, S., Kajino, T., Mathews, G.J., Otsuki, K. 2001, *ApJ*, 554, 578
- Wanajo, S., Tamamura, M., Itoh, N., Nomoto, K., Ishimaru, Y., Beers, T.C., Nozawa, S. 2003, *ApJ*, 593, 968
- Wasserburg, G.J., Qian, Y.-Z. 2000, *ApJ*, 529, L21
- Wheeler, J.C., Sneden, C., Truran, J.W. 1989, *ARA&A*, 27, 279
- Woolf, V.M., Tomkin, J., Lambert, D.L. 1995, *ApJ*, 453, 660
- Woosley, S.E., Hoffman, R.D. 1992, *ApJ*, 395, 202
- Woosley, S.E., Howard, W.M. 1978, *ApJS*, 36, 285

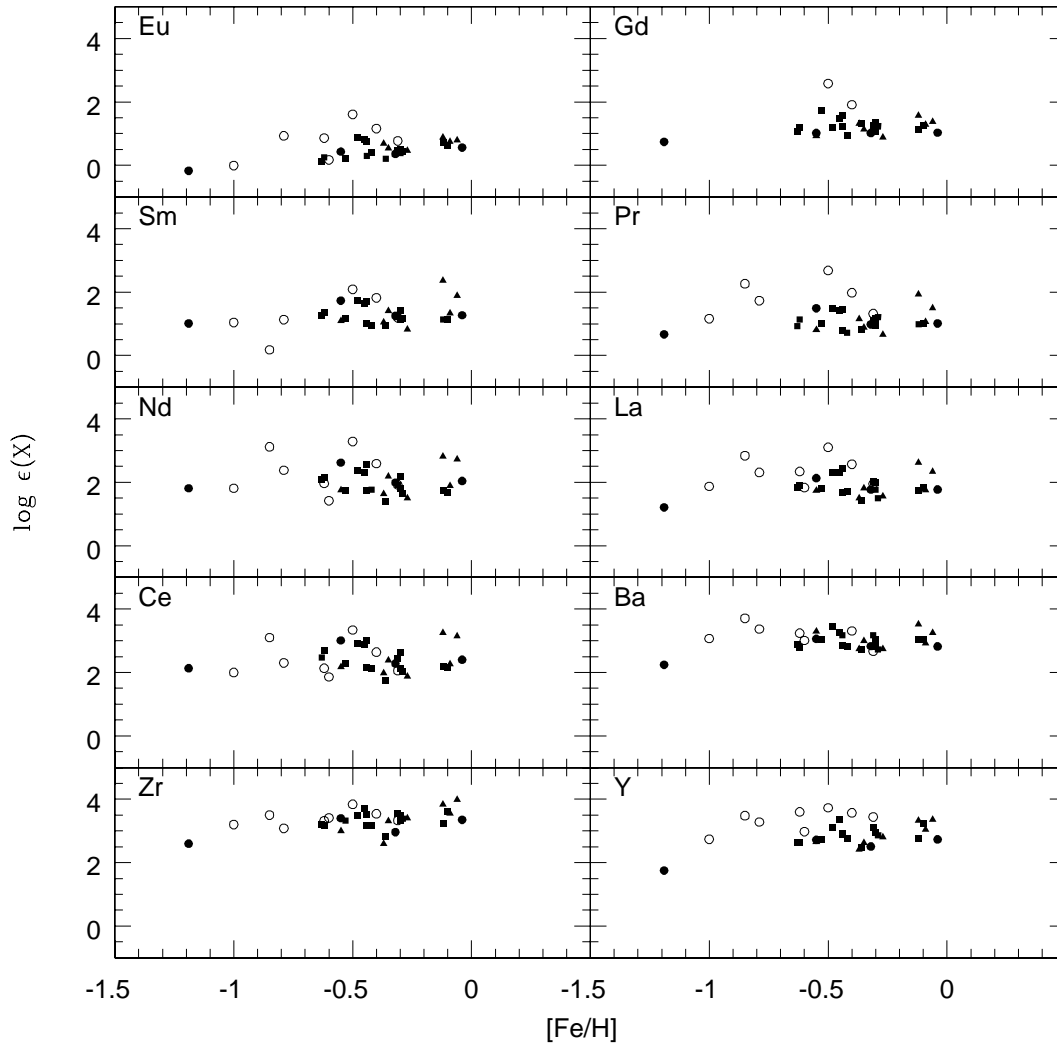


Fig. 7. $\log \epsilon(X)$ vs. $[\text{Fe}/\text{H}]$ for present sample barium stars and post-AGBs from Reyniers et al. (2004) and van Winckel & Reyniers (2000). Filled symbols indicate barium stars: squares: $\log g \geq 3.7$; triangles: $2.4 < \log g < 3.7$; circles: $\log g \leq 2.4$. Open circles are post-AGBs.

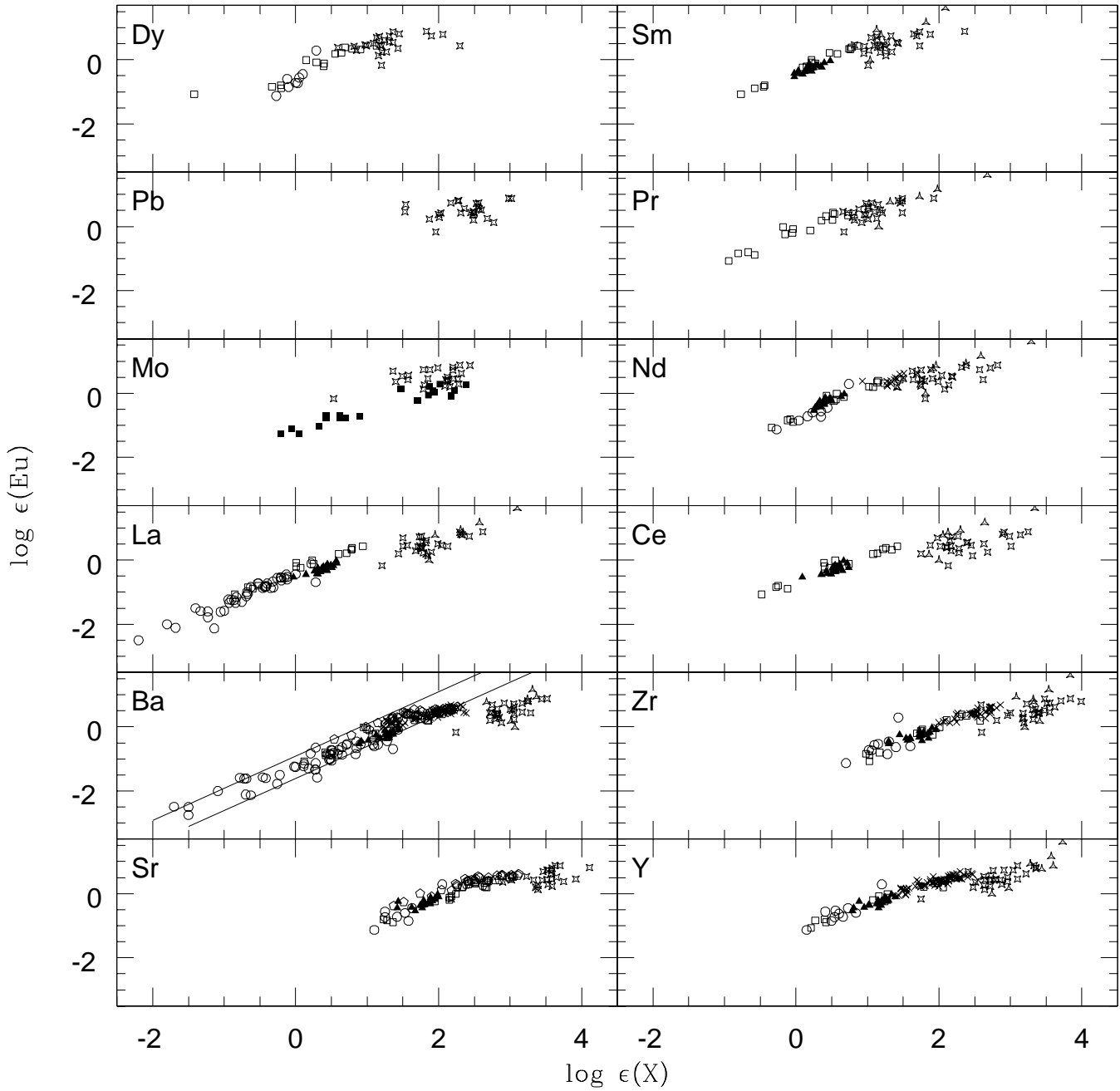


Fig. 8. $\log \epsilon(\text{Eu})$ vs. $\log \epsilon(X)$ for normal, post-AGB and barium stars. Normal stars from the literature are represented by symbols as in Figure 1. Starred squares are the present sample barium stars. Starred triangles are post-AGB from Reyniers et al. (2004) and van Winckel & Reyniers (2000). Solid lines in the Ba panel represent r-only production of Ba (upper line) and solar [Ba/Eu] (lower line).

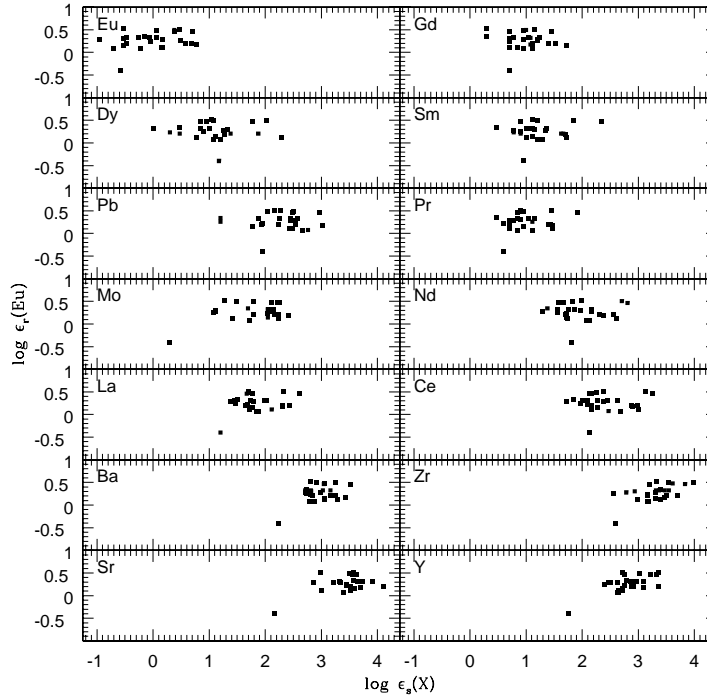


Fig. 9. $\log \epsilon_r(\text{Eu})$ vs. $\log \epsilon_s(X)$, where $\log \epsilon_r(\text{Eu})$ is the abundance fraction due to r-process for Eu and $\log \epsilon_s(X)$ is that due to s-process main component for other heavy elements in barium stars.

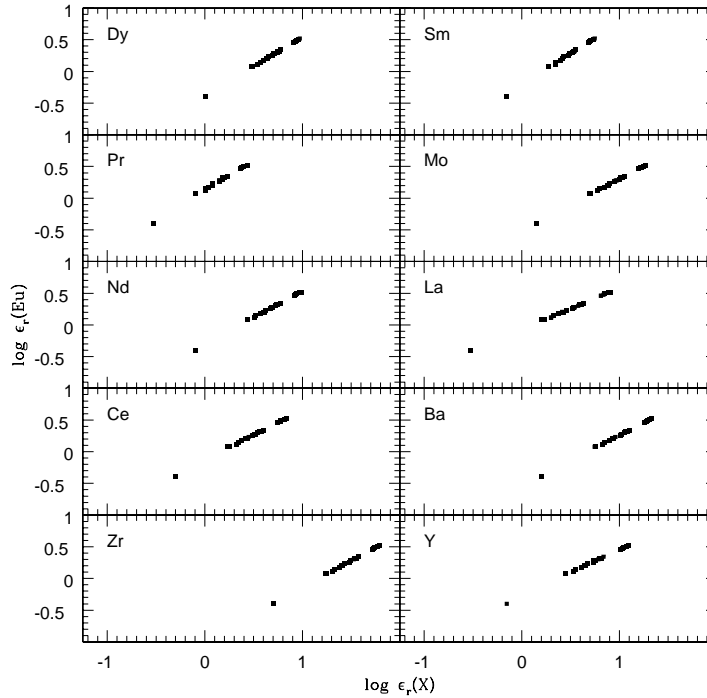


Fig. 10. $\log \epsilon_r(\text{Eu})$ vs. $\log \epsilon_r(X)$, where $\log \epsilon_r(\text{Eu})$ and $\log \epsilon_r(X)$ are the abundance fractions due to r-process for Eu and other heavy elements in barium stars, respectively.

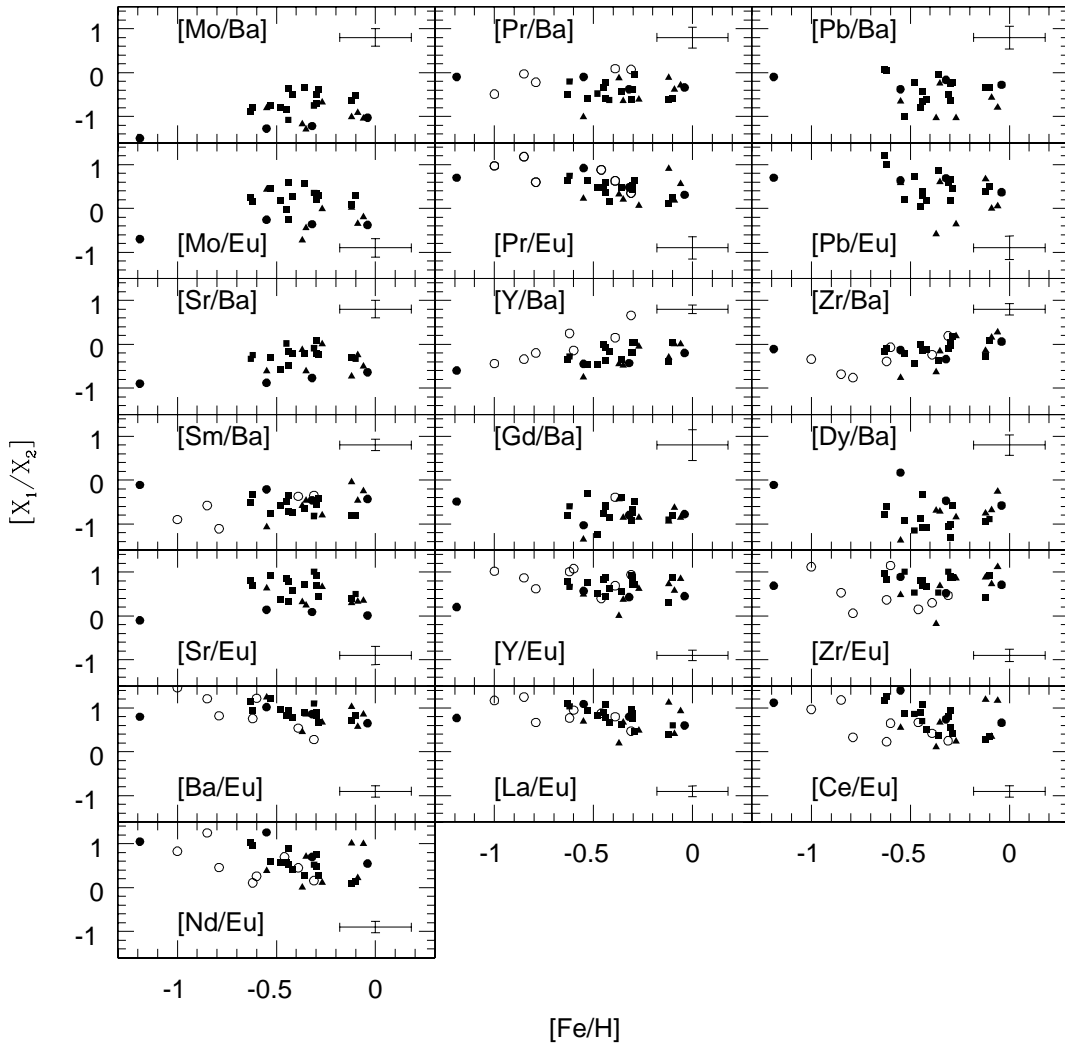


Fig. 11. Abundance ratios involving s- and r-processes, light and heavy s-elements. Uncertainties indicated are the largest values of Table 7 for each panel. Symbols are the same as in Figure 7.

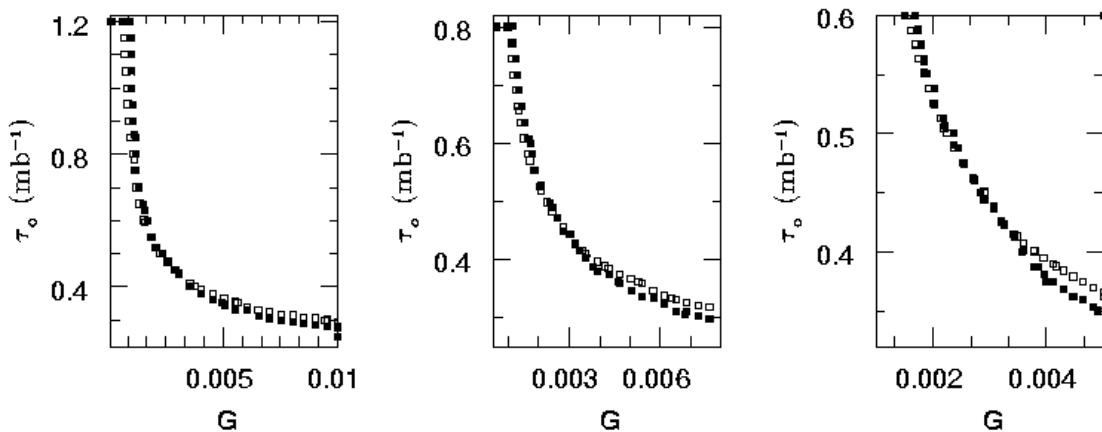


Fig. 16. Example of fit of parameters G and τ_0 for the barium star HD 123585. Open symbols correspond to the use of $\frac{\partial \chi}{\partial G} = 0$ and filled symbols, $\frac{\partial \chi}{\partial \tau_0} = 0$. From left to right the plot is zoomed in order to better visualize the crossing of the two functions.

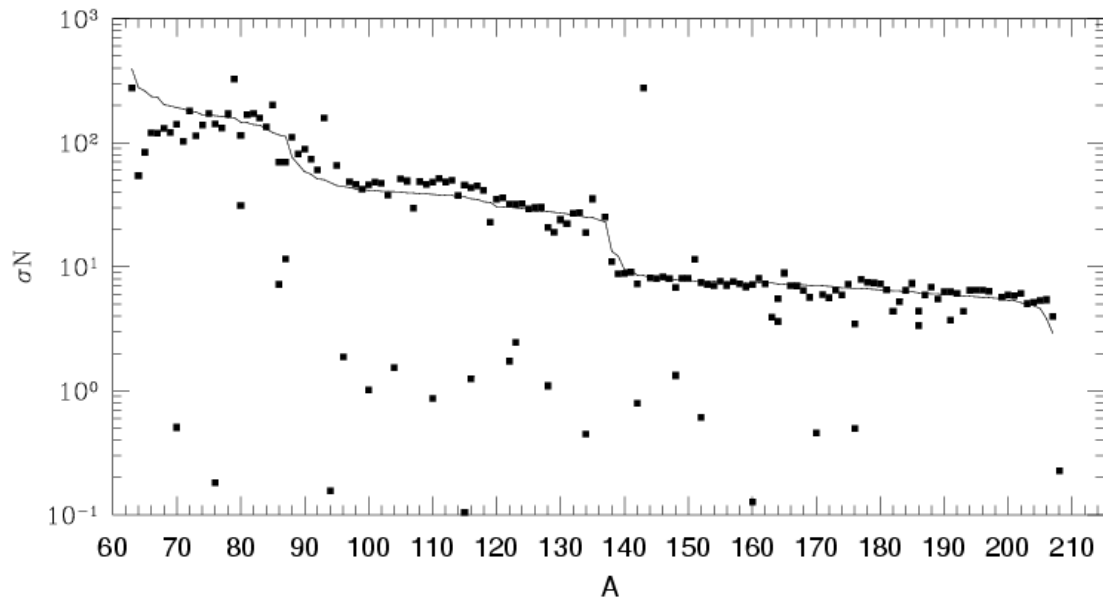


Fig. 17. Solar σN curve. Abundances related to s-process main component were taken from Arlandini et al. (1999).

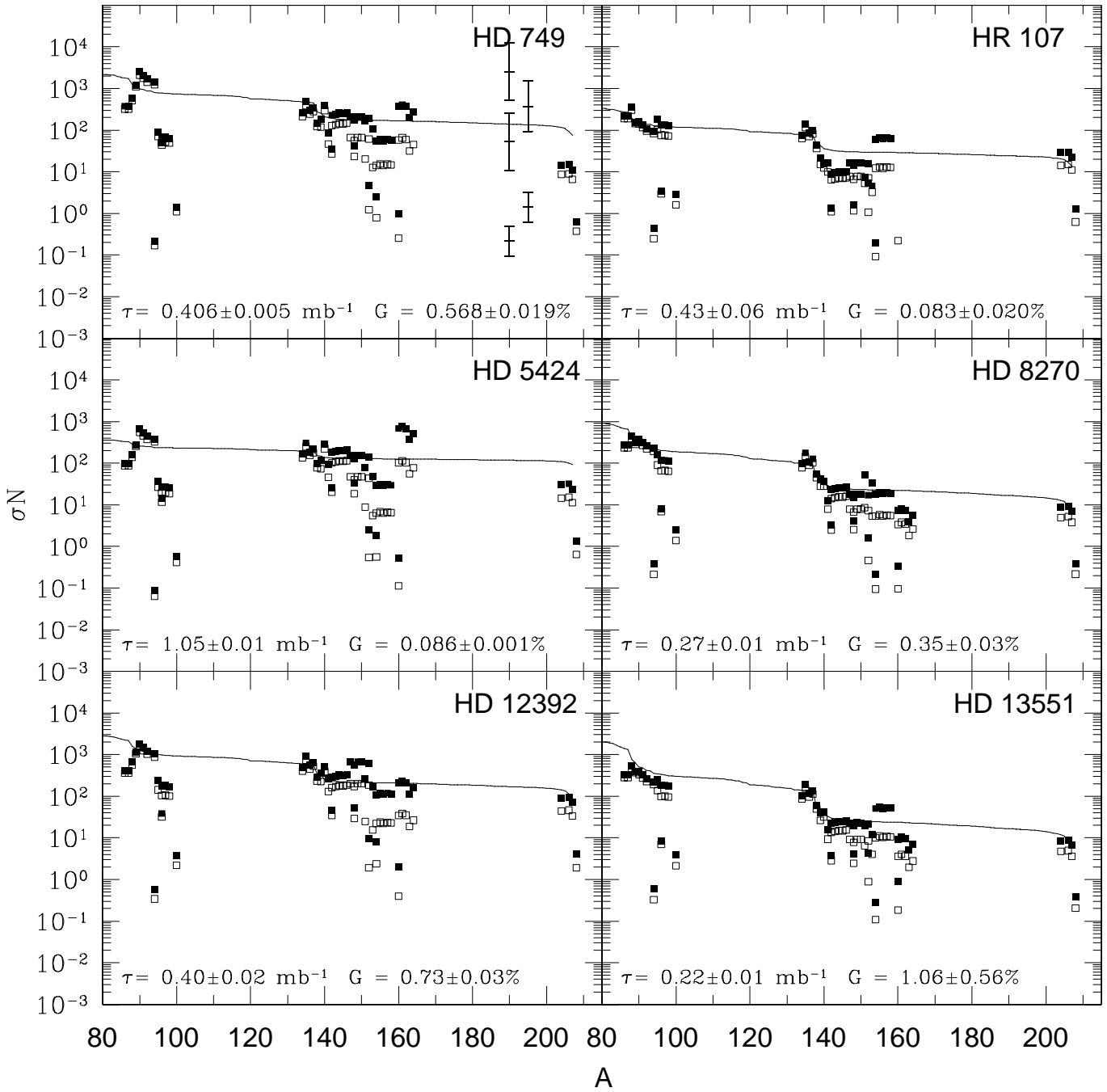


Fig. 18. σN curves for sample barium stars. Open squares represent solar distribution of abundances (column 18 of Table 6) and filled squares represent the distribution taking into account the overabundance of barium stars (column 16 of Table 6). Error bars in the HD 749 panel at $A=190$ and $A=195$, indicate the typical errors in each region of the logarithmic scale.

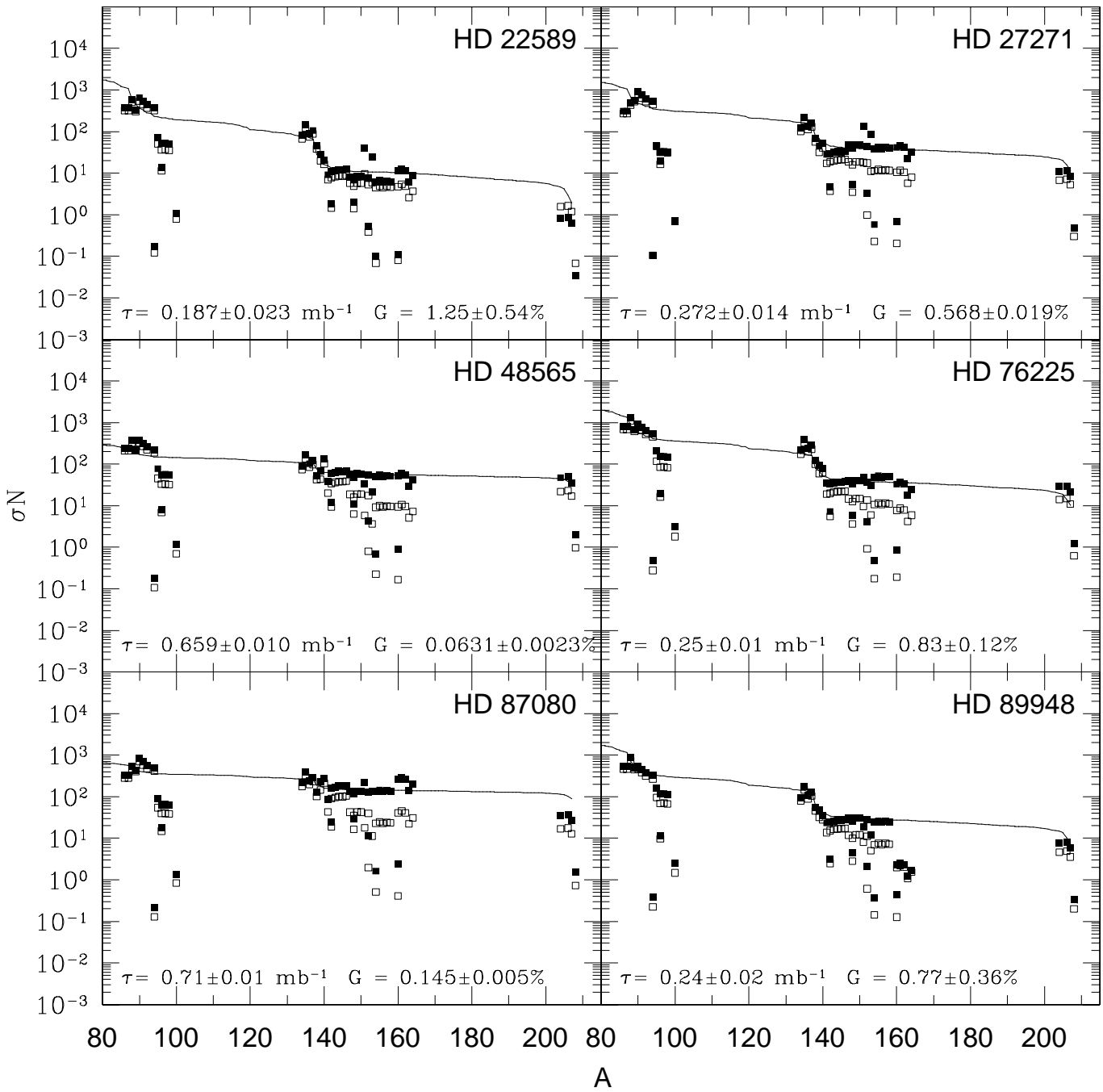


Fig. 19. Same as Figure 18 for other 6 sample stars.

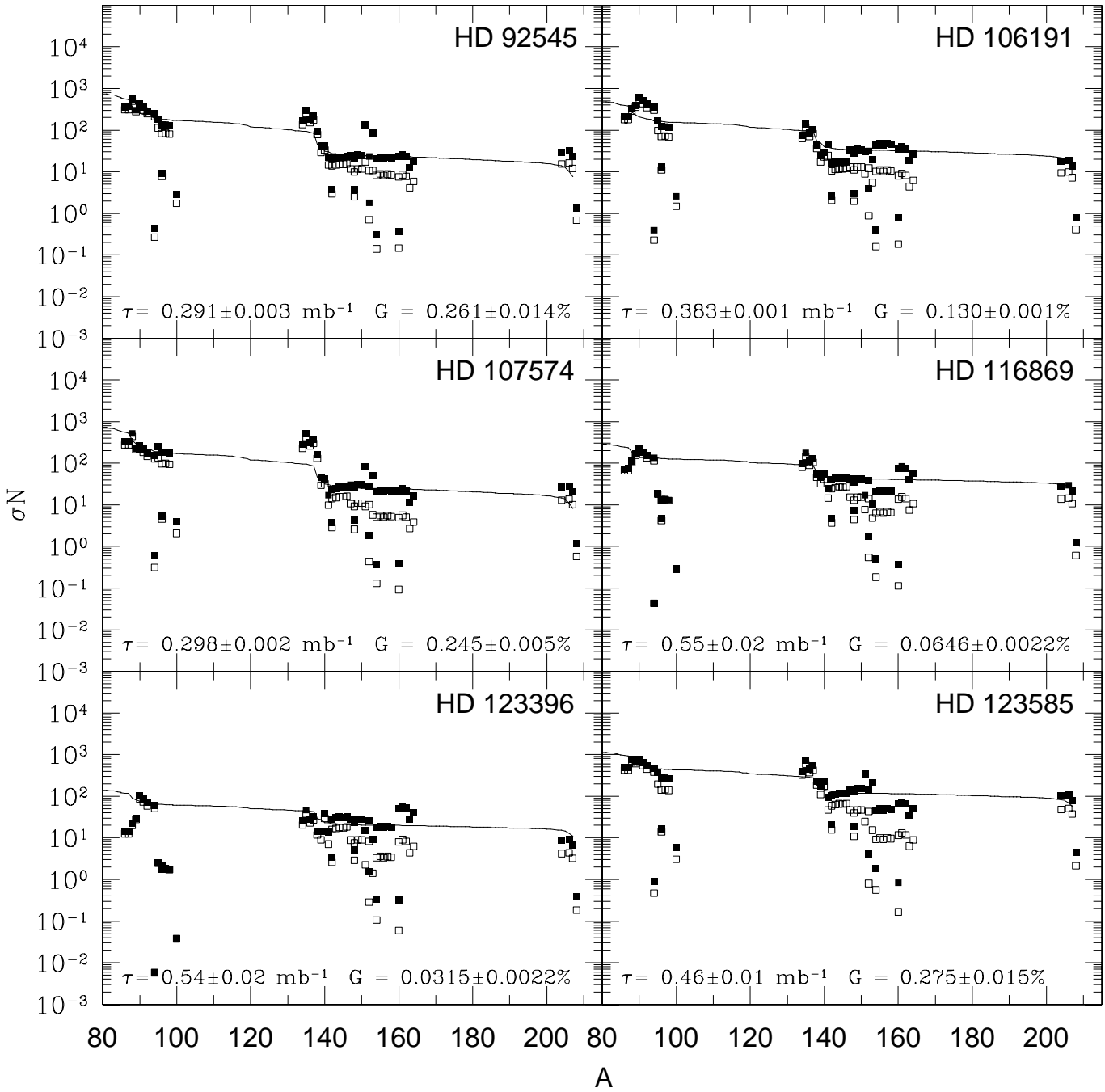


Fig. 20. Same as Figure 18 for other 6 sample stars.

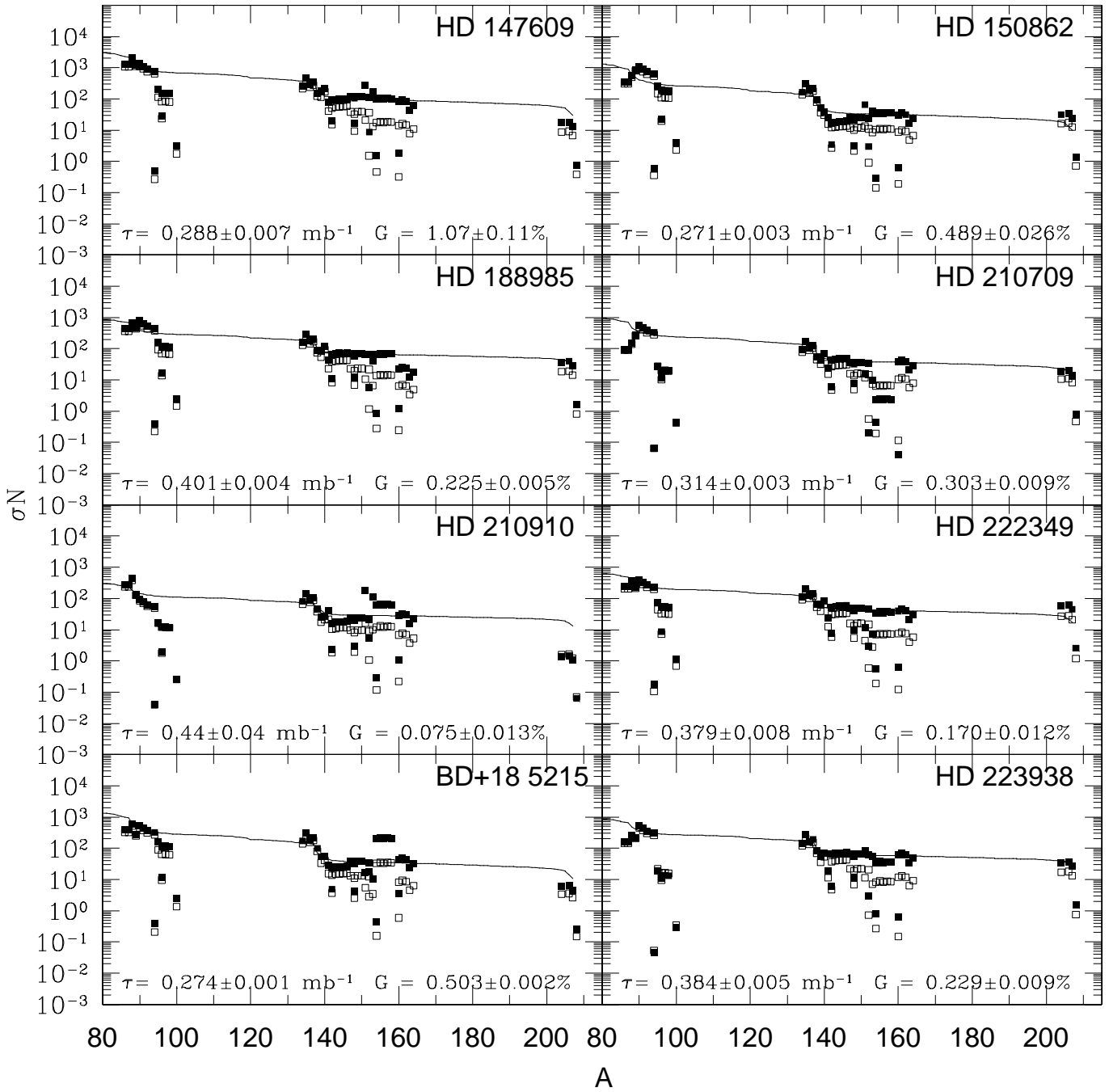


Fig. 21. Same as Figure 18 for other 8 sample stars.

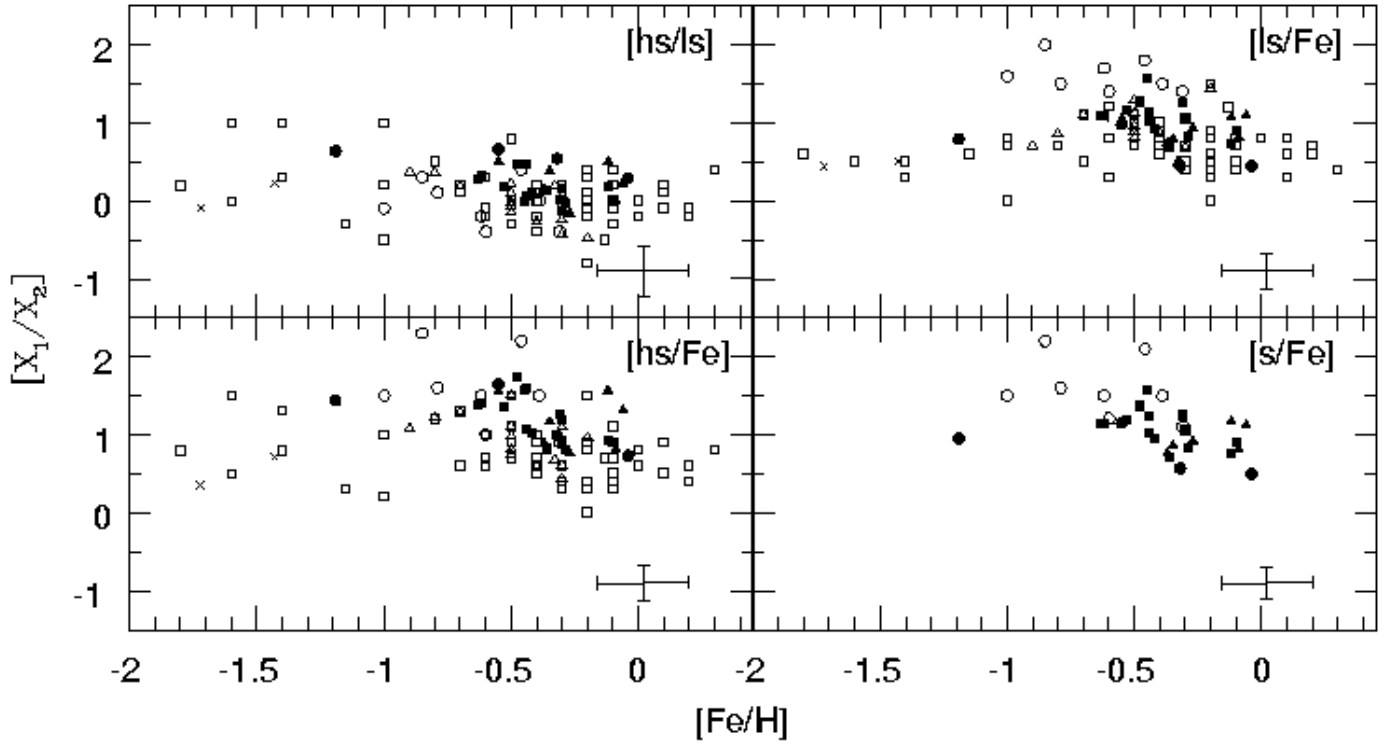


Fig. 22. $[hs/ls]$, $[ls/Fe]$, $[hs/Fe]$ and $[s/Fe]$ vs. $[Fe/H]$. Filled symbols indicate barium stars, as in Figure 7; open circles are post-AGBs; crosses are data from Junqueira & Pereira (2001); open squares are data from Luck & Bond (1991); open triangles are data from North *et al.* (1994). The uncertainties indicated are the higher values shown in Table 9.